Molecular and Dissociative Hydrogen Adsorption on Bimetallic PdAg/Pd(111) Surface Alloys: A Combined Experimental and Theoretical Study

Luis A. Mancera, Thomas Diemant, Axel Groß, and R. Jürgen Behm*

ABSTRACT: Aiming at a systematic, quantitative understanding of the surface chemistry of bimetallic PdAg surfaces, as present in bimetallic PdAg catalysts, we have investigated the adsorption of hydrogen on structurally well-defined PdAg/Pd(111) surface alloys by a combination of density functional theory (DFT)-based electronic structure calculations and temperature-programmed desorption (TPD) measurements. By comparison of experimental TPD data and calculated adsorption energies and making use of results of previous high-resolution scanning tunneling microscopy (STM) measurements (*Phys. Chem. Chem. Phys.* **2012**, *14*, 10754−10761, DOI: 10.1039/C2CP41104K), we could quantitatively correlate changes of the adsorption energy with increasing Pd content, as indicated by the formation and disappearance of additional desorption features in the TPD spectra, with the occupation of specific, mono- and bimetallic adsorption sites and ensembles on the PdAg surface. The results of this combined approach lead to a detailed understanding of the different effects affecting the hydrogen adsorption behavior on these bimetallic surfaces. Comparing the present results with previous findings for CO adsorption on similar PdAg surfaces and for hydrogen adsorption on PdAu/Pd(111) surface alloys allows us to place the resulting trends into a more general perspective, which is highly relevant also for the atomic-scale mechanistic understanding of catalytic reactions on bimetallic catalysts, specifically on a PdAg catalyst.

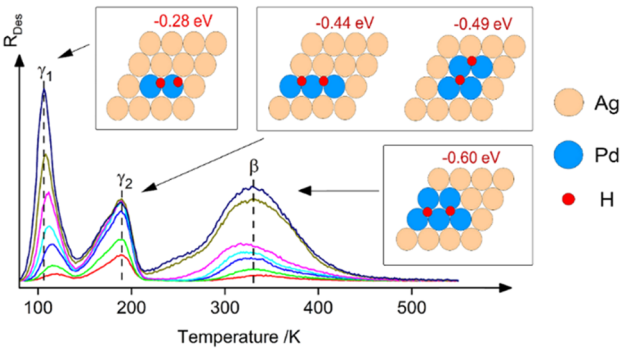

1. INTRODUCTION

Bimetallic catalysts have long been demonstrated to often exceed the respective pure components in their catalytic performance, which has been exploited in a number of catalytic or electrocatalytic reactions.[1,2] The improved performance has been explained to result from an interplay between different competing effects, including electronic ligand and strain effects and the geometric ensemble effect,[3−7] and this has also been accepted.[8,9] The different contributions to the overall performance of these catalysts however rely heavily on the distribution of the different components in the catalyst nanoparticles, both laterally, i.e., in the surface layer, and vertically, in particular in the near surface region. Therefore, varying the composition and the distribution of the components in a controlled way should not only allow to tune the desired reactivity and selectivity but also result in a quantitative understanding of the different contributions.

Among the various possible bimetallic systems, PdAg catalysts are particularly interesting due to their relevance with respect to catalytic reactions involving hydrogen, in particular for selective hydrogenation reactions[10−13] but also for electrocatalytic oxygen reduction.[14−16] Furthermore, bulk PdAg membranes were used as hydrogen separation membranes.[17,18] These potential applications led to a number of model studies on the surface composition[19−22] and adsorption behavior[23,24] of PdAg alloys. Interaction of hydrogen with pure Pd surfaces has also been a subject of intensive studies,[25−38] and the insights gained in these studies may also be relevant for the understanding of the catalytic properties of bimetallic PdAg systems interacting with hydrogen.

Studies employing structurally well-defined bimetallic model systems such as surface alloys can help to get a better

understanding of the chemical properties of bimetallic catalysts.[39,40] For this type of bimetallic system, a 2D bimetallic alloy layer is formed on a host metal. While the composition and distribution of the two metal components can be elucidated by high-resolution scanning tunneling microscopy (HR-STM), the underlying host metal can be considered to be uniform. This allows a straightforward correlation of changes in the chemical (adsorption/reaction) properties with variations in the abundance of specific surface nanostructures. The lateral distribution of the component atoms in the surface layer of PdAg/Pd(111) surface alloys was characterized for a number of different Pd concentrations by Engstfeld et al.[41] in a detailed analysis of STM images. Here it should be noted that based on those STM data, we can essentially exclude thermally or chemically induced local distortions or reconstruction of these surfaces under present experimental conditions, which also essentially excludes penetration of H_{ad} atoms into subsurface sites via such defects. Furthermore, the preparation and characterization of these surface alloys and their interaction with CO and O were studied before by Ma et al.[42,43] and Farkas et al.,[44] respectively, using temperature-programmed desorption (TPD), X-ray photoelectron spectroscopy (XPS), and high-resolution electron energy loss spectroscopy (HREELS). Later, we investigated the energetics and chemical properties of bimetallic PdAg/Pd(111) surface alloys by density functional theory (DFT) calculations, using adsorption of CO as a probe of the local adsorption behavior.[45] On the basis of the Sabatier principle, where the adsorption energy is used as a measure of the reactivity in a catalytic reaction, this may also serve as a measure for the catalytic performance.

In the present contribution, we address the adsorption of hydrogen on PdAg/Pd(111) surface alloys using a combination of DFT calculations and TPD measurements. This differs from the adsorption of CO since the dissociative adsorption of H_2 requires two H adatoms to be accommodated, and we expect that H_{ad} species are unlikely to diffuse over patches of pure Ag surface atoms, similar to observations for PdAu/Pd(111) surface alloys.[46,47] This assumption will be confirmed later in this study by the calculated difference in the H adsorption energies of about 1 eV (see below) for adsorption on Pd and Ag surface sites, which provides a lower bound for the diffusion barrier toward the Ag patches and clearly excludes any H_{ad} migration to these areas. Furthermore, the hydrogen adsorption energy on a specific two-dimensional (2D) Pd_xAg_y cluster may be a better measure for the local activity of this cluster in a hydrogenation reaction than the adsorption energy of CO. In our study, we make use of previously reported results on the 2D distribution of Pd and Ag surface atoms in these surface alloys, obtained for different Pd concentrations from HR-STM measurements.[41] In the TPD experiments, we used deuterium gas (D_2) instead of H_2 to obtain a better background discrimination. It may be noted that the total adsorption energy calculated by DFT does not depend on the isotope, as the mass of the nucleus does not affect the electronic interaction, while zero-point and vibrational entropy effects depend on the mass. Still, the use of D_2 instead of H_2 was found to result only in a small change of the experimentally observed adsorption energy.[48] In the DFT calculations, we focus on the determination of the site specific hydrogen adsorption energies on different Pd_n ensembles and on the effect introduced by inhibiting H_{ad} transport between individual Pd_n ensembles, which means that adsorption of H_{ad} is only possible in a pairwise mode, to accommodate both H_{ad} species resulting from an adsorbing H_2 molecule. To account for effects introduced by subsurface Ag, we also included pseudomorphic Pd_xAg_{1-x} surface alloys with a pseudomorphic Ag layer underneath and a closed Pd cover layer supported on a pseudomorphic Ag subsurface layer on Pd(111), in addition to pure pseudomorphic Pd_xAg_{1-x}/Pd(111) monolayer surface alloys. Finally, we compare our results with those obtained for the closely related system of PdAu/Pd(111) surface alloys, which we had investigated recently in a comparable approach.[47]

The remainder of this paper is organized into five sections: In section 2, we describe the main experimental and computational details of our study. Section 3.1 presents the pertinent results of the D_2-TPD measurements from Pd_xAg_{1-x}/Pd(111) surface alloys with different compositions, while in section 3.2, we present results of the theoretical modeling of H adsorption, H_2 adsorption, and H_2 dissociation using DFT-based electronic structure calculations. Here, we will make use also of the different models introduced for explaining trends in the adsorption energies on bimetallic surfaces (ensemble, ligand and strain effect). In section 4, we discuss our main experimental and theoretical results and findings, comparing in particular TPD results and calculated adsorption energies. Finally, we present our conclusions in section 5.

2. EXPERIMENTAL AND COMPUTATIONAL DETAILS

2.1. Experimental Details. The experiments were performed in an ultra-high-vacuum (UHV) system (base pressure < 1×10^{-10} mbar), which is equipped with facilities for X-ray photoelectron spectroscopy (XPS) and temperature-programmed desorption (TPD) measurements. The PdAg/Pd(111) surfaces were prepared following a similar procedure as in previous studies.[41,42] The Pd(111) single crystal was cleaned by Ar^+ ion sputtering (5 min, ~1 μA, 0.9 kV) at room temperature (RT), oxygen treatment (5 min, $p_{O_2} = 1 \times 10^{-7}$ mbar) at 900 K, and final annealing to 1100 K. STM measurements on a similarly prepared and cleaned Pd(111) single crystal have shown atomically flat terraces with a width of 50−200 nm.[41] Ag was deposited with a rate of ~0.05 ML min^{-1} on the Pd(111) surface at RT using a resistively heated Knudsen cell (WA technology). To reduce contributions from the backside of the crystal in the subsequent TPD measurements, it was covered by a closed Ag layer. The PdAg/Pd(111) surface alloys were prepared by an annealing step to 800 K (for 60 s). It is well-known that this annealing step leads to the loss of Ag into the bulk of about ~10−15% for Ag coverages up to 0.8 ML.[41,42] This loss increases for higher initial Ag coverages, and even after deposition of thick Ag layers, it is impossible to reach surfaces compositions with very high Ag/very low Pd surface concentration (>90% Pd). To prepare such surfaces, it is necessary to reduce the annealing temperature. In the present study, for the surface with the highest Ag surface concentration, the heating step after deposition of ~1.5 ML Ag was limited to 650 K (60 s). The surface composition of the alloys was determined by XPS measurements using the $I_{Ag(3d)}/I_{Pd(3d)}$ intensity ratio, which was cross-calibrated to the results of CO TPD measurements, taking advantage of the fact that the relation of the CO_{ad} saturation coverage with the surface composition of the PdAg/Pd(111) surface alloys is already known.[43]

For the TPD experiments, the D_2 exposure was performed by backfilling the chamber via a glass tube (inner diameter 8 mm) pointing toward the sample (distance to the glass tube: ~50 mm). Deuterium gas (D_2) was used instead of hydrogen for better background discrimination. H_2 and D_2 have the same electronic structure but differ in mass by a factor of 2. If the sticking process is dominated by electronic excitations in the solid, then both molecules should feature a very similar sticking probability. The thermodynamic dissociation or binding energy of D_2 is larger than for the H_2 molecule by −0.08 eV due to vibrational zero-point energies; the difference in adsorption energy may even be smaller.[48] Calibration measurements revealed that the actual pressure at the sample position was about two times that measured at the ion gauge. Therefore, all pressure and exposure values were corrected for that. Exposure started at a sample temperature of 90 K, during adsorption it continued to decay to 80 K. Subsequently, a linear heating ramp of 4 K s^{-1} was applied and the D_2-TPD spectra were recorded with a quadrupole mass spectrometer (Pfeiffer Vacuum, QMS 200). The mass spectrometer was shielded against desorption from the sample edges by a cap with an aperture of 4 mm diameter. Before a TPD run, the sample was positioned in front of the aperture, and the distance between cap and sample was adjusted by an electrical contact, which resulted in very reproducible absolute intensities of the TPD spectra.[49] Additional TPD measurements, following a nearly similar procedure, were performed on PdAg/Pd(111) surfaces prepared in another way. To create these surfaces, a closed Ag layer (θ_{Ag} = 1.5 ML) was initially deposited on the Pd(111) substrate at RT and then gradually annealed to a stepwise increased temperature (in 50 K steps up to 1000 K). After each annealing step (and cooling back to 90 K), D_2-TPD spectra were collected (the exposure was limited to 20×10^{-6} mbar s^{-1} to keep the background level low; ~95% of the saturation coverage is reached after this exposure).

2.2. Computational Details. For the calculations we used settings and notation similar to those used in our previous study of PdAg/Pd(111) surface alloys.[45] All calculations were performed using version 4.6 of the VASP code,[50] together with the Perdew−Burke−Ernzerhof (PBE)[51] exchange-correlation functional. The ion cores were represented by projector augmented wave (PAW) potentials.[52] as constructed by Kresse and Joubert.[53,54] The electronic one-particle wave functions were expanded in a plane-wave basis set up to a cutoff energy of 400 eV. Spin polarization was not considered due to the non-spin-polarized nature of the system. A dipole moment correction was included in order to account for effects arising from using asymmetric slabs. Scalar relativistic effects were not explicitly considered in the periodic DFT calculations; however, they were taken into account in the construction of the PAW potentials. Convergence criteria for the electronic self-consistency and the ionic relaxation were set to 1×10^{-5} and 1×10^{-4} eV, respectively. Energy barriers between the initial and final position of H atoms were calculated for some particular cases based on the nudged elastic band (NEB) method.[55,56] For that, we used eight images along each path and interpolated the results using a cubic spline algorithm. In this case, the convergence criteria for the electronic self-consistency and the ionic relaxation were set to 1×10^{-4} and 1×10^{-3} eV, respectively, i.e., one order of magnitude larger than for the other calculations. The exact location of the transition state is then identified by testing whether all forces vanish at this saddle point, and its energy is checked by a single-point calculation. Adsorption energy values reported were obtained using a (3×3) unit cell with a $3 \times 3 \times 1$ Γ-centered *k*-point grid to represent the surfaces. This *k*-point grid is known to yield reliable results within the DFT accuracy.[45] In all cases, they refer to the energy of H_2 molecules in the gas phase. As a consistency check, we compared calculations using a larger unit cell (5×5) with a $2 \times 2 \times 1$ Γ-centered *k*-point grid, having approximately the same density of *k*-point in reciprocal space. Here, also the hydrogen coverages are different. For adsorption of one hydrogen atom per unit cell, i.e., in the low coverage limit, both unit cell sizes are assumed to result in similar adsorption energies. Calculations for the two different unit cell sizes indeed yielded rather similar results, suggesting that these calculations are indeed reliable with respect to the *k*-point sampling and are representative for the low-coverage limit. The bimetallic surfaces were represented by periodic slabs consisting of five monolayers. Geometry optimization of the various surface configurations was performed by keeping the two bottom Pd(111) layers fixed at their corresponding bulk positions, while the three upper layers were fully relaxed. Ag_{nL}/Pd(111) denotes a structure with *n* pseudomorphic silver overlayers above the Pd(111) substrate, Pd_{mL}/Ag_{nL}/Pd(111) denotes a structure with *m* pseudomorphic palladium overlayers and *n* pseudomorphic silver sublayers above the Pd(111) substrate (the total number of layers is still limited to 5), Pd_xAg_{1-x}/Pd(111) denotes a surface alloy at the topmost layer, and Pd_xAg_{1-x}/Ag_{nL}/Pd(111) denotes a structure with a surface alloy at the topmost overlayer and *n* pseudomorphic silver layers underneath.

3. RESULTS

3.1. Experimental Results. *3.1.1. STM Analysis of the PdAg/Pd(111) Surfaces.* Before presenting the D_2-TPD results, we briefly summarize the most important results of the structural characterization of the PdAg/Pd(111) surface alloys by high-resolution STM performed in a previous study.[41] Atomically resolved STM pictures were recorded for various surface alloy compositions, and their digitized versions were used to derive the atom distribution and the lateral short-range order, and to investigate ensemble and ligand effects. First, it may be noted that a pseudomorphic surface alloy layer is formed for all Ag contents without any evidence for a reconstruction. From a first visual inspection of the STM images, there is no observable short-range order in the surface alloy layer. This impression was confirmed by a statistical evaluation of the images using the Warren−Cowley coefficients as parameters for the short-range order. For all compositions, the alloy layers are close to a random distribution, although a slight preference for homoatomic clustering in the nearest-neighbor sphere was derived for smaller Ag contents (x_{Ag} < 45%) and a preference for unlike neighbors for higher Ag contents (x_{Ag} > 65%). This is also reflected in the ensemble statistics, i.e., the abundance of different small Pd ensembles in the alloy surfaces (Pd_2, Pd_3, etc.), which follows more or less the development expected for a random distribution.[41] This means for Ag-rich surface alloys that only Pd monomers in a surrounding of Ag atoms are found up to a surface concentration of ~5% Pd. At ~10% Pd, some isolated Pd_2 ensembles (dimers) can also be found, but the majority of the Pd atoms are still monomers. Finally, for a Pd surface content above 20% also larger Pd ensembles (trimers of different shape, etc.) appear. This trend was also corroborated by a combination of CO TPD and vibrational spectroscopy

measurements,[43] where the latter can differentiate between adsorption on Pd monomers (on-top adsorption), dimers (adsorption on bridge sites), and trimers (adsorption on 3-fold-hollow sites).

3.1.2. D_2-TPD from Well-Defined PdAg/Pd(111) Surfaces. Here we present the results of TPD measurements after D_{ad} (adsorbed D atom) saturation of PdAg/Pd(111) surface alloys with different Ag contents and, for comparison, that of pure Pd(111). These results will later be related to the results of the DFT calculations in section 3.2, a comparison to adsorption on other similar bimetallic systems will follow in section 4. TPD spectra recorded after a D_2 exposure of 60×10^{-6} mbar s are shown in Figure 1. This exposure proved to be sufficient to

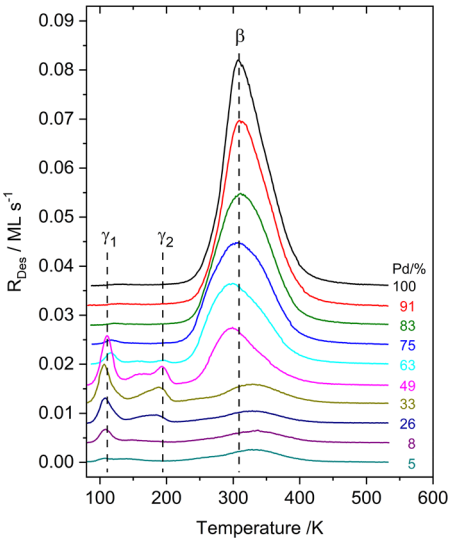

Figure 1. D_2-TPD spectra after D_{ad} saturation of pure Pd(111) and various PdAg/Pd(111) surface alloys with decreasing Pd content (from top to bottom). We denote the three peaks as γ_1 (at ∼120 K), γ_2 (at ∼195 K), and β (at ∼310 K).

saturate all investigated surfaces. The exposure was started at 90 K (and the temperature typically decreased to ∼80 K during exposure). Gdowski et al. showed that at these temperatures the rate for subsurface absorption of hydrogen through the Pd(111) surface into the Pd bulk is rather low[29] and that the use of deuterium instead of hydrogen reduces this tendency further.[30] The D_2-TPD spectrum of pure Pd(111) shows a slightly asymmetric peak with a maximum at ∼310 K, which was denoted as β peak previously.[29] Our results are in good agreement with previous reports on H_2 desorption from Pd(111).[29,30,47,57] Upon saturation of the Pd(111) surface, adsorbed hydrogen forms an (1 × 1) adlayer structure,[25,28] corresponding to a saturation coverage of 1 ML.

With increasing Ag (and therefore decreasing Pd) surface content, the intensity of the main desorption peak quickly diminishes, so a surface with 26% Pd content reaches a minimum value of ∼7% of the initial intensity for pure Pd(111). This residual desorption signal remains unchanged for samples with larger Ag content, even for a sample with a closed Ag layer on the Pd substrate. Therefore, this residual signal is most probably due to deuterium desorption from the sides of the crystal, which were not passivated when covering the crystal backside by a closed Ag layer. It may be noted that this residual signal even amounted to ∼17% of the initial intensity when the backside was not passivated by a Ag layer. The continuous decrease of the D_{ad} saturation coverage with increasing Ag surface content clearly indicates that stable adsorption of D_{ad} on (pure) Ag ensembles is unlikely under these conditions, a conclusion which is corroborated by our DFT calculations (see below). Apart from the decrease of its intensity, we also find a slight shift (by ∼10 K) of the β peak maximum toward lower temperatures with increasing Ag surface content, as long as the main peak can be safely discerned from the background contribution. We tentatively attribute this shift to the electronic ligand and strain effects in the surface alloy, which modify the local D_{ad} adsorption properties. Additionally, adsorbate−adsorbate interactions may also affect the adsorption behavior at high coverages. In any case, none of these changes is very pronounced.

With increasing Ag surface content, additional desorption features can be observed at lower temperatures (see Figure 1). This starts out as a very small peak at 120 K for a PdAg surface with 75% Pd. This feature, which we call γ_1 peak, grows very quickly with increasing Ag surface content and shifts by ∼10 K toward lower temperatures. It reaches its maximum intensity for a surface with 49% Pd and decreases again for larger surface Ag contents. At the same composition (49% Pd), another feature (γ_2 peak) appears at higher temperature. It consists of a peak at 195 K with a shoulder at lower temperature (∼170 K). Similar to the γ_1 peak, it also decreases in intensity with increasing Ag surface content. When comparing the development of the two γ peaks, we note that the γ_2 peak disappears faster with increasing Ag/decreasing Pd content than the γ_1 peak. While the γ_2 feature is already absent in the D_2-TPD spectrum for the surface with 8% Pd, the γ_1 peak disappears completely only for a surface with 5% Pd.

The γ_2 feature is in the temperature range where desorption from subsurface sites was reported to occur for Pd(111) after hydrogen exposure at higher temperature (>120 K).[29,58] Furthermore, based on DFT calculations, Ozawa et al.[59] concluded that for a (111) surface the subsurface/bulk adsorption of hydrogen should be more facile for a Pd_3Ag bulk alloy than for pure Pd, due to the larger lattice constant of PdAg alloys compared to Pd. In fact, a similar result was also reported by Noordermeer et al.,[57] who compared the hydrogen uptake of a $Pd_2Ag(111)$ bulk alloy and a Pd(111) single crystal in TPD experiments. In our case, with a PdAg pseudomorphic alloy monolayer on the Pd(111) substrate, such effects are unlikely, since there is no lattice expansion. We therefore exclude the possibility that the features at low temperatures are due to deuterium desorption from subsurface sites. Furthermore, the fact that the γ peaks saturate already after relatively small D_2 exposures also disfavors the occupation of subsurface/bulk sites.

Most likely, these additional desorption features at low temperatures are either due to H_{ad} desorption from (bimetallic) sites with a significantly lower binding energy and/or due to strongly repulsive H_{ad}−H_{ad} interactions. The latter may result also in the occupation of other adsorption sites (hcp, bridge, and top). Weak bonding on bimetallic sites such as Pd_2Ag or even $PdAg_2$ trimers seems to be most likely. This will be discussed in more detail in section 4 when comparing our experimental TPD results to the DFT calculations.

The development of D_{ad} saturation coverage with decreasing Pd content in the overlayer is plotted in Figure 2. The residual D_{ad} coverage of 0.07 ML in the β peak, which was observed for Ag-rich Pd_xAg_{1-x}/Pd(111) surface alloys and which we

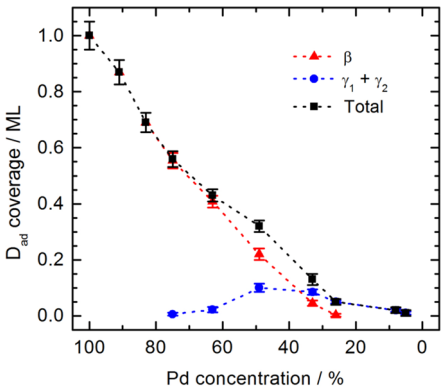

Figure 2. D_{ad} saturation coverage on PdAg/Pd(111) surface alloys (black squares). Desorption intensity in the main β peak (red triangles) and in the γ features (γ_1 + γ_2, blue circles). For a better visualization of the trends, we connect the symbols with dashed lines.

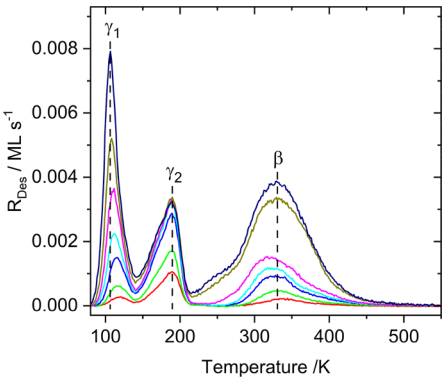

Figure 3. D_2-TPD spectra of a $Pd_{33}Ag_{67}$/Pd(111) surface alloy after increasing D_2 exposures (from bottom to top: 0.1, 0.2, 0.4, 0.6, 1, 20, and 60 × 10 ^{6} mbar s).

attributed to undesired contributions from the side of the crystal, was removed for the calculation of the D_{ad} coverages for all data points shown in this figure. Obviously, the decrease of the total D_{ad} coverage with decreasing Pd content in the surface layer is not linear. For the β peak, it decreases very quickly with a nearly linear behavior and approaches zero for a surface alloy with 26% Pd (after subtraction of the background intensity). In fact, an extrapolation of the initial slope reaches zero D_{ad} coverage already at 40% Pd surface concentration. In contrast, the intensity of the γ peaks first increases for surfaces with intermediate Pd contents, reaching 0.1 ML for a $Pd_{49}Ag_{51}$/Pd(111) surface alloy and then decreases again, reaching, e.g., 0.05 ML for an alloy with 26% Pd. At higher Ag content, the total D_{ad} coverage, which contains mainly the γ peaks contributions, decreases further, reaching 0.02 and 0.01 ML for alloys with 8 and 5% Pd, respectively. In the latter case, no clear peak can be identified anymore and the integrated intensity results just from a very low desorption intensity over the whole range of the γ features. For a closed Ag layer on Pd(111), i.e., directly measured after Ag deposition, the integrated desorption intensity in the whole temperature range equals ∼0.005 ML D_{ad} and is completely due to undesired background contributions.

The evolution of the D_2-TPD spectra with increasing D_2 exposure for surfaces with intermediate Ag content, where the low-temperature γ peaks are most pronounced, is illustrated for the $Pd_{33}Ag_{67}$/Pd(111) surface alloy in Figure 3. Here, we focus on the two γ peaks, which show an interesting behavior: These two peaks appear and grow already at very low exposures, long before saturation of the β peak. Apparently, the adsorption sites corresponding to these two peaks are populated at the same time as those related to the β peak and not sequentially, as would be expected from an energetic point of view. Furthermore, the γ_2 peak at 175 K seems to grow faster at low exposure, while the γ_1 peak at 125 K grows faster at higher exposure. These results can most easily be explained if the different peaks are due to desorption from isolated adsorption sites, e.g., from small Pd_n ensembles, which are separated by weakly binding Ag atoms. This inhibits D_{ad} diffusion to more stable adsorption sites, and D_{ad} species must be accommodated on the Pd_n ensemble where they adsorb initially. A similar phenomenon was observed also for H_2 adsorption on PdAu/Pd(111) surface alloys.[47] Furthermore, the faster initial growth of the γ_2 peak compared to the γ_1 peak points to a higher sticking coefficient on the sites related to the γ_2 peak, which results in earlier saturation, while the sites related to the γ_1 state require larger exposure to reach saturation. The higher final intensity of the γ_1 state is simply due to the higher number of such sites on this surface. Finally, it is important to stress that each of these isolated adsorption sites has to accommodate an even number of hydrogen adatoms, since diffusion of one of the two atoms of a hydrogen molecule away to another stable site during adsorption or desorption is inhibited.

3.1.3. D_2-TPD: Effect of the Annealing Temperature. In the following, we describe an experiment in which first a closed Ag adlayer (θ_{Ag} = 1.5 ML) was deposited on the Pd(111) substrate at RT, leading to a $Ag_{1.5\ ML}$/Pd(111) surface, which was subsequently annealed to increasingly higher temperature to create PdAg/Pd(111) surface alloys. This is different from the previous experiments (section 3.1.2), where all surfaces alloys were obtained by depositing different amounts of Ag atoms and then annealing to a fixed temperature of 800 K. In the present experiments, in contrast, we start with a fixed initial Ag coverage and then gradually anneal the surface to a stepwise increased temperature (in 50 K steps up to 1000 K). After each annealing step and cooling, the resulting surface was exposed to D_2, and then D_2-TPD spectra were collected (the exposure was started at 90 K again and limited to 20 × 10^{-6} mbar s to keep the background level low; ∼95% of the saturation coverage was reached after this exposure). The results of this experiment are shown in Figure 4.

The first TPD spectrum (bottom) results from D_2 desorption of the $Ag_{1.5\ ML}$/Pd(111) surface before annealing. It shows weak D_2 desorption in the range of the β peak, which we attribute to desorption from the crystal sides. Apart from that, no other features are detected until the sample is annealed to 700 K. At this point, the γ_1 peak appears for the first time with very low intensity (∼0.01 ML D_{ad}). Its intensity increases after every annealing step and amounts to ∼0.03 ML D_{ad} after heating to 800 K. After heating to 900 K, the γ_2 desorption feature is detected for the first time. The increase of the desorption intensity of the β peak after the next annealing step (950 K) indicates the appearance of Pd ensembles with similar desorption characteristics as an unmodified Pd(111) surface. At this point, the γ features have reached their maximum intensity. The last heating steps (to 1000 and 1100 K) lead to the complete disappearance of the γ peaks and to a significant further increase of the β peak intensity. For the highest annealing temperature, the D_2-TPD spectrum is identical to

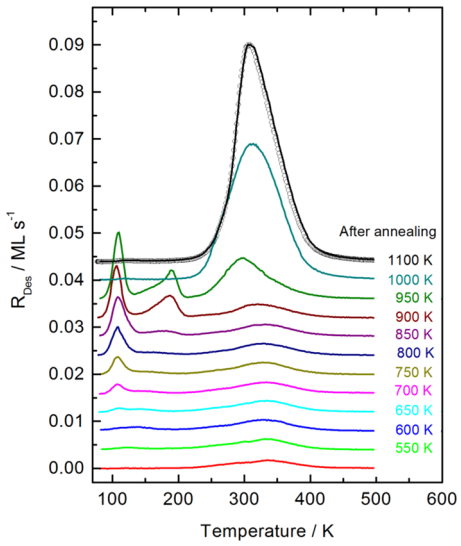

Figure 4. D_2-TPD spectra of PdAg/Pd(111) surface alloys obtained from a progressively annealed initial $Ag_{1.5\ ML}$/Pd(111) surface. Each spectrum is recorded after annealing (in 50 K steps up to 1000 K) and after D_2 exposure (20×10^{-6} mbar s) at 90 K. The spectrum at the bottom corresponds to the surface before annealing.

that of pure Pd(111), which was recorded the same day before Ag deposition (see Figure 4, open circles).

A similar type of experiment was performed before by Ma et al.[42] to characterize the surface alloy formation process after Ag deposition on Pd(111), using a combination of XPS, TPD, and vibrational spectroscopy measurements with CO as probe molecule. While initially, after Ag deposition at RT, a closed Ag layer is present on the surface, annealing to increasing temperature causes more and more Pd atoms to segregate to the surface, although the Pd surface content must be rather low after the first annealing steps. Ma et al. determined the Pd concentration from the measured CO_{ad} saturation coverage. For low Pd surface contents, they assumed a 1:1 ratio between CO and Pd sites, with CO adsorbed on isolated Pd surface atoms and Pd dimers in the Ag matrix. With the formation of larger contiguous Pd ensembles after annealing to higher temperature, repulsive CO_{ad}–CO_{ad} interactions come into play, and the maximum CO_{ad} coverage (per Pd atom concentration) converges to the CO saturation coverage of pure Pd(111). While the CO desorption signal was negligible for the closed Ag layer (Ag = 1.2 ML), they obtained a Pd coverage of ~7% after annealing this surface to 550 K. This is not surprising, since intermixing of Pd and Ag (surface alloy formation) starts already at a temperature as low as 450 K.[42] Up to 800 K, the increase of Pd content in the overlayer is rather slow (up to ~10% Pd). Beyond this point, the changes are much more pronounced, due to the onset of Ag desorption and enhanced diffusion into the bulk. Finally, after annealing to 1100 K, an essentially Ag-free surface is restored. For comparison, for a thicker initial Ag layer (θ_{Ag} = 3 ML), the Pd coverage was still negligible after annealing to 550 K and increased more steadily after that, leading to a similar situation (~10% Pd) after annealing to 800 K (and beyond that).

Furthermore, from the appearance of characteristic features in the CO-TPD spectra, Ma et al. could identify the formation of different adsorption ensembles.[42] While the Pd atoms are initially isolated and CO adsorption is on top of these atoms, Pd_2 ensembles bind CO_{ad} in a bridge configuration with a slightly higher CO binding strength. An additional CO molecule can be bound on the Pd_2 ensembles, but it desorbs at much lower temperature, due to the strongly repulsive CO_{ad}–CO_{ad} interactions. The desorption signal of this second CO_{ad} molecule on a Pd_2 dimer is a diagnostic for the formation of these sites, it is detected for the first time after annealing the surface to 800 K. After annealing the sample to 900 K, the desorption peak characteristic for CO from compact Pd_3 sites (Pd_3-c) is observed in the CO-TPD spectra. Annealing to 1100 K leads eventually to a CO-TPD spectrum, which is very similar to that of pristine Pd(111). These experimental results for CO adsorption on PdAg/Pd(111) were fully supported and clarified by a subsequent DFT study of our group.[45]

The findings of our measurements shown in Figure 4 can be compared with the results of Ma et al.,[42] which allows us to correlate the appearance of the γ and β peaks with the Pd ensembles formed with increasing annealing temperature. The absence of any peak after the first annealing steps, in the temperature range where CO adsorption was possible (450–750 K) on Pd monomers, clearly demonstrates that deuterium adsorption on Pd monomers (or on larger mixed ensembles containing a single Pd surface atom) is not possible under present experimental conditions (minimum temperature 80 K). After annealing at 800 K, the surface alloy should contain already ~10% Pd in the surface layer. The γ_1 peak in our D_2-TPD spectra (at 120 K) can be assigned to desorption from Pd_2 sites, since it appears as the first desorption state after annealing to 700 K and becomes very prominent after heating to 800 K. The intensity of the γ_1 peak and hence the number of Pd_2 ensembles is still rather low after annealing to 700 and 750 K. Therefore, the Pd_2 ensembles may have been overlooked in the CO-TPD measurements by Ma et al.,[42] since the desorption peak of the second CO_{ad} molecule appears as a low temperature shoulder to the main desorption peak. The γ_2 peak instead is likely correlated with the occurrence of larger Pd ensembles, like Pd_3 surface sites or even Pd_4 ensembles, while the β peak requires most probably the formation of Pd_5 and larger ensembles. This assignment is completely corroborated by the DFT calculations presented in the next chapter.

3.2. Computational Results. In order to better understand and interpret the experimental findings presented in section 3.2, we performed periodic DFT calculations of the adsorption energies of H atoms on PdAg/Pd(111) surface alloys. For comparison, we also calculated adsorption energies of H atoms on the pure Pd(111) surface, on a Pd(111) surface terminated with pseudomorphic silver or palladium/silver overlayers, and on PdAg surface alloys with underlying pseudomorphic silver layers. In addition, we studied the effect of molecular H_2 adsorption, which considering that diffusion over pure Ag surface areas is strongly hindered means that each Pd ensemble needs to accommodate an even number of H adatoms, and discuss the possible consequences of that boundary condition. We are particularly interested in the energetics obtained for the adsorption of two H atoms on a Pd surface ensemble, to gain insight into the role played by the size of the Pd ensembles in the dissociation of the adsorbing H_2 molecule, which will be used for comparison with the experimental data.

3.2.1. The H/Pd(111) System. Table 1 shows adsorption energies of H atoms on a pure Pd(111) surface at different H_{ad} coverages, which compare favorably with previously published results.[32] For all coverages, adsorption occurs preferentially at

Table 1. Adsorption Energies of H on Pd(111) as a Function of H_{ad} Coverage[a]

	PBE/PAW		
θ_H	1/9	1/3	2/3
T	−0.06	−0.03	0.00
fcc	**−0.63**	**−0.61**	**−0.57**
hcp	−0.59	−0.56	−0.52
B	−0.48	−0.46	−0.40

[a]T, fcc, hcp, and B denote top, fcc-hollow, hcp-hollow, and bridge sites, respectively. Values are given in eV/adatom, calculated using PBE/PAW in a 3 × 3 unit cell. Bold values denote the preferential adsorption sites for all coverages.

the fcc-hollow sites (see Table 1). Adsorption at the on-top sites is energetically feasible only for low H_{ad} coverage. Adsorption at the bridge site does not correspond to a local minimum, i.e., it is not stable. In order to obtain an adsorption energy value for the bridge site, the lateral coordinates of the H adatom were fixed. Adsorption at a bridge site is 0.1−0.2 eV weaker than for the hollow sites, depending on the type of hollow site and the H_{ad} coverage.

The bridge site corresponds to the transition state for hydrogen diffusion along the diffusion path hcp−bridge−fcc, as we have confirmed using NEB calculations for θ_H = 1/9, plotted in Figure 5. Since adsorption on the fcc site is more

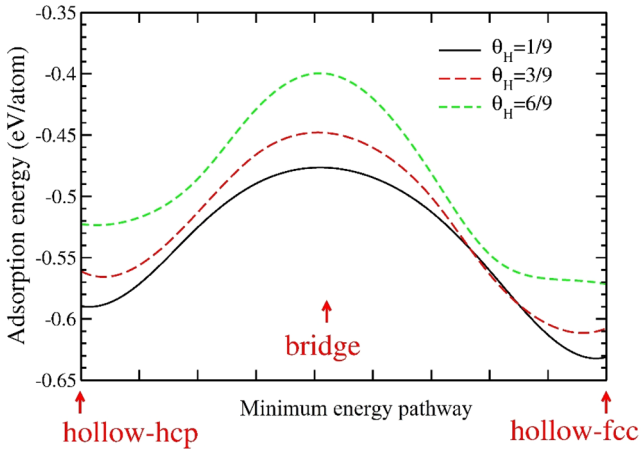

Figure 5. NEB calculation for H adatom diffusion on a clean Pd(111) surface along the pathway from an hcp-hollow site via a bridge site to an fcc-hollow site. Values were calculated using a 3 × 3 unit cell and three different H_{ad} coverages ($^1/_9$, $^3/_9$, and $^6/_9$). At the latter two coverages, all H adatoms in the unit cell moved from the hcp to the fcc hollow sites along the diffusion pathway, keeping the distance between the migrating H adatoms essentially constant. Energies are given in eV/adatom and referred to the energy of the H_2 molecule in the gas phase.

favorable than on the hcp site, the barrier from the fcc to the hcp site (0.15 eV) is slightly higher than the barrier from the hcp to the fcc site (0.11 eV). These barriers depend rather weakly on H coverage, as demonstrated by the barriers for θ_H = $^1/_9$, $^1/_3$, and $^2/_3$ in Figure 5. The corresponding values for the hcp to fcc barriers are 0.11, 0.10, and 0.12 eV, in the reverse path they amount to 0.15, 0.15, and 0.17 eV, respectively.

A slight decrease of the H adsorption energy with increasing H_{ad} coverage is also observed in Table 1: At any surface site, the H adsorption energy decreases by 0.06 to 0.08 eV per H_{ad} atom for changes in the H_{ad} coverage in the range of θ_H = $^1/_9$−$^2/_3$. Since there is no difference in the preferred H_{ad} adsorption sites, this decrease is indicative of weakly repulsive H_{ad}−H_{ad} interactions. As evident from the curve profiles, the H−H repulsion is not constant along the trajectory, but larger around the bridge sites. For comparison, for CO adsorption the same change in CO_{ad} coverage induces a decrease in the adsorption energy between 0.4 and 0.6 eV.[45] There is a small change of the adsorption site symmetry (lateral displacement) also for H_{ad}, but this is much less pronounced as the one observed for CO molecules.[45]

3.2.2. The H/Pd_{mL}/Ag_{nL}/Pd(111) System. To test for the hydrogen adsorption energies on extended Ag overlayers and for the influence of subsurface Ag on the adsorption of H_{ad} on Pd surface ensembles we performed calculations with one H atom per (3 × 3) surface unit cell on pseudomorphic Ag or Pd/Ag layers deposited on Pd(111). This corresponds to a low H_{ad} coverage of $^1/_9$. The adsorption energies obtained for the different adsorption sites are collected in Table 2. On the

Table 2. Adsorption Energies of a H Atom on Pseudomorphic Ag and Pd/Ag Overlayers on Pd(111) at a H_{ad} Coverage of θ_H = 1/9[a]

	PBE/PAW		
	$Pd_{1L}/Ag_{1L}/Pd_{3L}$	$Pd_{1L}/Ag_{2L}/Pd_{2L}$	Ag_{1L}/Pd_{4L}
T	0.04	0.22	0.67
fcc	**−0.72**	**−0.50**	0.27
hcp	−0.71	−0.48	0.29
B	−0.54	−0.33	0.46

[a]See Table 1 for comparison with pure Pd(111). T, fcc, hcp, and B denote top, fcc-hollow, hcp-hollow, and bridge sites, respectively. Values in eV/atom, calculated using PBE/PAW in a 3 × 3 unit cell. Bold values denote the preferential adsorption sites in each case.

pseudomorphic silver layer (Ag_{1L}/Pd_{4L}) as the topmost layer, all the adsorption energies are positive, which means that the adsorption is unstable with respect to associative desorption. The same is true for Ag_{2L}/Pd_{3L}, Ag_{3L}/Pd_{2L}, and Ag_{5L} (not reported in the table), and the results are similar to the H adsorption energies on pure Ag(111).[60] Different from the structures with Pd bottom layers, the Ag_{5L} structure was calculated with the two bottom layers fixed to the silver lattice parameter, while the upper layers were relaxed.

However, if a pseudomorphic Pd layer is added above the silver layers, then H adsorption occurs at hollow sites, and for the case of $Pd_{1L}/Ag_{1L}/Pd_{3L}$, those H adsorption energies can even be stronger than for a pure Pd(111) surface. This trend, which has also been observed for adsorption on Pd/Au[61] and Pt/Au systems[62] can be explained by the (vertical) ligand effect, which can also be explained via bond-order arguments.[9] Since the Pd surface layer is not so strongly bound to the underlying Ag layer as to a Pd substrate, it can therefore bind adsorbates more strongly. These considerations can also be explained within the d-band model.[33]

For two Ag underlayers below the Pd surface layer, however, the binding of the adsorbate becomes weaker. This trend can also be explained in a bond-order picture. Now the Ag layer below Pd is less strongly bound to the underlying second Ag layer, which results in a stronger interaction with the uppermost Pd layer, which then consequently binds adsorbates more weakly. Interestingly, this line of arguments does not explain that H adsorption is weaker on the $Pd_{1L}Ag_{2L}Pd_{2L}$

surface than on Pd(111), indicating that other effects play a role as well.

Similar to our above observations for Pd(111), adsorption on the bridge site is not stable for all cases reported in Table 2. Therefore, the adsorption energy on these sites was obtained using constrained coordinates as explained above in order to keep the H atom in the bridge position, otherwise it would migrate to a neighboring hollow site. The interaction of H atoms at the top sites is always weaker than that at the hollow sites and unstable against associative desorption under present experimental conditions. In this latest case, it was not necessary to constrain the coordinates of the H atom to keep it on the top site, since during the relaxation it moves away from the surface. Hence, rather than migrating to the hollow site, it desorbs. Finally, when comparing H to CO adsorption, energy differences between top and hollow sites are significantly larger than the corresponding energy differences for adsorbed CO molecules.

3.2.3. The H/PdAg/Pd(111) System. Next we calculated H_{ad} adsorption energies on PdAg/Pd(111) surface alloys. Table 3

Table 3. Adsorption Energies of a H Atom on a PdAg/Pd(111) and a PdAg/Ag_{1L}/Pd(111) Surface Alloy Considering Pd_1, Pd_2, Pd_3, and Pd_4 Ensembles[a]

		PBE/PAW	
	site	PdAg/Pd_{4L}	PdAg/Ag_{1L}/Pd_{3L}
Pd_1	T	−0.04	0.03
	fcc*	**−0.15**	**−0.12**
	hcp*	−0.11	−0.12
Pd_2	T	−0.06	0.09
	B	**−0.43**	**−0.25**
	fcc*	−0.17	−0.10
	hcp*	−0.13	−0.10
Pd_3-c	T	−0.06	0.12
	fcc	**−0.60**	**−0.30**
	hcp	−0.49	−0.29
	fcc*	—0.18/—0.39	—0.09/—0.17
	hcp*	—0.13/—0.16	—0.04/—0.09
Pd_3-1	T	−0.05	0.11
	B	**−0.45**	**−0.26**
Pd_3-b	T	−0.06	0.12
	B	−0.43	−0.20
	fcc*	**−0.45**	**−0.21**
Pd_4	T	−0.04	0.12
	fcc	**−0.58**	**−0.29**
	hcp	−0.51	−0.29
	fcc*	—0.19/—0.43	—0.06/—0.19
	hcp*	−0.16	−0.04

[a] Pd_3-c, Pd_3-l, and Pd_3-b denote compact, linear and bent Pd_3 ensembles, respectively. T, fcc, hcp, and B indicate top, fcc-hollow, hcp-hollow, and bridge sites, respectively. Different from the case of H adsorption on clean Pd surfaces, we did not constrain the H atoms at the perfect bridge sites. Bold values highlight the preferential adsorption sites in each case. Sites marked with an asterisk describe hollow positions around the ensemble. H_{ad} coverage is 1/9. Values are given in eV/atom, calculated using PBE/PAW in a 3 × 3 unit cell. For a visual description of the H adsorption configurations, see Figure 6.

shows values computed for a (3 × 3) unit cell, at a H_{ad} coverage of $\theta_H = {}^1/_9$. In these calculations, we consider the most compact ensembles, i.e., Pd_1 monomers, Pd_2 dimers, compact triangular Pd_3 trimers (Pd_3-c), and a rhombic Pd_4 tetramer. For Pd_3, we also considered two additional less compact structures, namely, a linear (Pd_3-l) and a bent (Pd_3-b) ensemble. For H adsorption, we considered both sites involving only Pd atoms and sites where H_{ad} resides on mixed clusters such as Pd_1Ag_2. The different H adsorption configurations are presented in Figure 6. This graph also contains the adsorption energies obtained for the different pure and mixed adsorption sites.

In the following, we will discuss the general trends indicated by these calculations. In that discussion, the changes in the local binding strength will be discussed considering geometric ensemble effects, indicated by the different sites (on top, bridge, and hollow sites) as well as electronic ligand and strain effects.[9,46,47,63,64] In fact, we will demonstrate that these three effects together with bond-order arguments are fully sufficient to reconcile the trends found in the DFT calculations. When replacing a Pd atom in the uppermost layer by a Ag atom, the ligand effect makes the Pd atoms adjacent to the inert Ag atom more reactive, due to the weaker bond between Ag and Pd as compared to Pd−Pd interaction (bond-order argument). In contrast, Ag atoms are larger than Pd atoms, and replacement of Pd by a Ag surface atom effectively leads to a compressive strain which lowers the interaction strength of the adjacent Pd atoms with adsorbates.[45] Similar effects had been reported for PdAu/Pd(111),[47,63,65] PtRu/Ru(0001),[66−68] and PtAu/Au(111)[62] surface alloys. In the latter case, it was found that these effects nearly cancel, keeping the adsorption strength at Pt sites nearly independent of the surface alloy composition.[62]

There is a variety of sites on the PdAg/Pd_{4L} surface alloys that in principle allow H adsorption at temperatures above 100 K, i.e., with adsorption energies exceeding 0.35 eV. Nevertheless, reaching an adsorption energy similar to that for adsorption at hollow sites of the Pd(111) surface (−0.63 eV) is only possible for adsorption on compact Pd trimers, i.e., at fcc-hollow sites in the inner part of the larger ensembles (Pd_3-c and Pd_4). Furthermore, adsorption at the top, bridge, and hollow sites that are exclusively coordinated to Pd atoms and leads to adsorption energies very similar to those on the corresponding sites on Pd(111) (see Table 1). These results clearly indicate that the counteracting effects of ligand and strain effects effectively cancel each other also on PdAg/Pd_{4L} surface alloys.

Looking at the trends in more detail, we find for adsorption on Pd_1 monomers that adsorption on top of the Pd monomer is very weak, similar to our findings for H adsorption on Pd(111), and this is also true for all ensembles discussed in the following. Instead, the H atom adsorbs preferentially at the hollow sites formed by the Pd_1 monomer and the two neighboring Ag surface atoms, i.e., on a Pd_1Ag_2 hollow site. This is more stable than adsorption on a bridge site (Pd_1Ag_1 site) or in an on-top configuration (Pd_1 site). In these mixed 3-fold-hollow sites, the H adatom is shifted from the symmetric position toward the Pd atom. Furthermore, adsorption is slightly stronger on the fcc-hollow site than on the hcp-hollow site. Nevertheless, in all cases the adsorption energy is below 0.2 eV; therefore, we do not expect stable adsorption on these sites at 100 K.

For Pd_2 dimers, the H atom adsorbs preferentially at the bridge site, but it does not remain exactly at the center of the

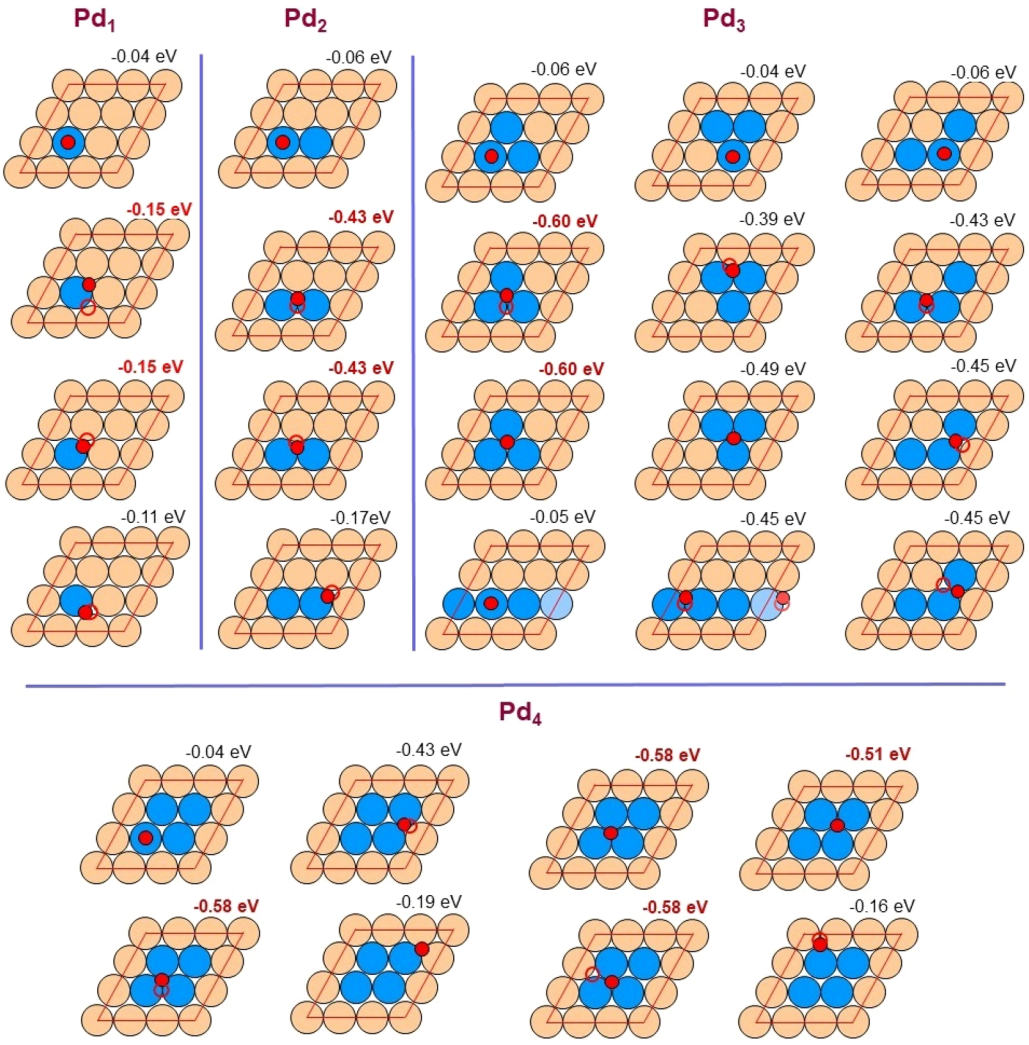

Figure 6. Adsorption of a single H atom on Pd_1, Pd_2, Pd_3, and Pd_4 ensembles of PdAg/Pd(111) surface alloys. Empty and filled red circles denote the initial and the final position of the H atom, respectively. Bold red values denote the largest adsorption energies in each case. Values are in eV/adatom, calculated using PBE/PAW in a 3 × 3 unit cell. Due to the periodicity of the unit cell, a linear Pd_3 ensemble leads to an infinite linear chain. In this case, periodic images of Pd and H atoms are represented with lighter colors.

bridge site, but instead tilts slightly to the neighboring fcc-hollow site. Hence, this can again be described as adsorption on a mixed ensemble, in this case on a Pd_2Ag_1 ensemble, with the H adatom displaced toward the Pd_2 bridge site. The same occurs if the H atom is first located at the hcp-hollow site in the middle part around the ensemble: upon relaxation it spontaneously migrates toward the bridge position tilted to the centered fcc-hollow site. This reveals again a different strength of the interaction at fcc-hollow and at hcp-hollow sites, similar to H adsorption on the clean Pd(111) surface (see Table 1). On the basis of the adsorption energy of around 0.4 eV, these sites could be populated at temperatures around 100 K. At the ends of the Pd_2 ensembles, an H adatom can adsorb at the surrounding fcc-hollow sites (Pd_1Ag_2 ensemble) with an adsorption energy of −0.17 eV, comparable to that for adsorption at the mixed fcc-hollow site around Pd_1 and thus too low to be populated at 100 K.

For a compact Pd_3 ensemble, the adsorption occurs preferentially at the inner hollow site, and it is stronger if that site is a fcc-hollow site (−0.60 vs −0.49 eV). Adsorption at the surrounding hollow sites involving one Ag atom, on mixed Pd_2Ag trimers, shows intermediate adsorption energies. There are, however, two different situations depending on the type of hollow site formed by the Pd_3 ensemble. If this is of fcc-hollow type, then a H atom adsorbs at the surrounding hollow sites at the corners with a rather weak adsorption energy (−0.18 eV for fcc-hollow and −0.16 eV for hcp-hollow), comparable to the situation for adsorption at hollow sites around Pd_1 and Pd_2 ensembles. Adsorption in hcp-hollow sites directly aside the Pd_3 ensemble is not possible, because the H atom migrates with no energy barrier toward the inner fcc-hollow site. The situation is different if the inner site of the Pd_3 ensemble is of the hcp type. In this case, the H atom can adsorb stably on the fcc-hollow sites aside the ensemble with an energy of −0.39 eV, and migration to the central hollow site of the Pd_3 ensemble is hindered by a barrier. Similar to our findings for the off-center bridge site on Pd_2 dimers this should be sufficient to stabilize adsorption at 100 K. In principle, the H atom could also adsorb at the outer hcp-hollow sites at the corners of the ensemble with an energy of −0.13 eV, which would, however, be too low to stabilize adsorption at 100 K.

For a linear Pd_3 ensemble, adsorption is preferred at the bridge site in a similar manner as for Pd_2, and the adsorption energy is also of comparable magnitude (−0.45 eV), enough to

stabilize adsorption at 100 K. Effects of mixed fcc- and hcp-hollow sites are also comparable to those for Pd_2 dimers.

For bent Pd_3 ensembles, adsorption occurs preferentially at a mixed Pd_2Ag_1 fcc-hollow site, tilted to the Pd_2 bridge. The adsorption energy is again around −0.45 eV. Upon adsorption on a bridge site or on a hcp-hollow site, the H adatom moves without a barrier to the asymmetric fcc-hollow site, reflecting the higher stability for adsorption on this site. All of these findings are comparable to the situation observed for adsorption on a Pd_2 dimer, and the same is also true for adsorption at the ends of the Pd_3 trimer (not shown in Figure 6).

For the compact Pd_4 tetramer, the strongest adsorption occurs at the inner fcc-hollow site (−0.58 eV), whereas at the inner hcp-hollow site it is slightly weaker (−0.51 eV). Adsorption on the mixed Pd_2Ag_1 hollow sites at the side of the Pd_4 tetramer is only possible at the fcc-hollow sites (−0.43 eV), whereas from the hcp-hollow sites the H adatom migrates to the neighboring inner fcc-hollow site. Finally, for adsorption on the mixed Pd_1Ag_2 sites located at the corners of the ensemble, an H atom can adsorb with energies of −0.19 and −0.16 eV at fcc-hollow and hcp-hollow sites, respectively, which are both too small to stabilize adsorption at 100 K.

In total, these calculations indicate that fcc-hollow adsorption sites are the preferred sites for H adsorption (with a shift toward the adjacent Pd atom(s) for mixed Pd_nAg_{3-n} ensembles), while the hcp-hollow adsorption sites show slightly lower adsorption energies. H adsorption occurs always on (asymmetric) hollow sites, with slightly lower adsorption energies for the hcp-hollow adsorption site. For Pd_3-type hollow sites, adsorption energies are around −0.6 to −0.65 eV, for mixed Pd_2Ag_1 type sites aside the ensembles the adsorption energies are around −0.45 eV, while for Pd_1Ag_2 sites the adsorption energies are too low to stabilize adsorption at 100 K. The same is true for adsorption on on-top sites, regardless of the size of the Pd ensemble.

Introducing one silver layer beneath the PdAg alloys generally leads to a weaker hydrogen binding, similar to our findings for CO adsorption.[64] H adsorption at the on-top sites of the various Pd ensembles, which is very weak for the PdAg/Pd(111) surface alloy, becomes completely unfavorable with silver sublayers. Differences in the H adsorption energy between PdAg/Pd(111) and PdAg/Ag_{1L}/Pd(111) can reach values up to ∼0.3 eV. This is at first surprising as hydrogen adsorption at the bridge and hollow sites on the Pd monolayer deposited on Ag_{1L}/Pd_{3L} is stronger than on Pd(111) (see Table 2). The reduction in the binding strength might be explained at least qualitatively in a similar way as the change in the adsorption energies between the $Pd_{1L}/Ag_{1L}/Pd_{3L}$ and the $Pd_{1L}/Ag_{2L}/Pd_{2L}$ system, using simple bond-order arguments: Upon introducing the Ag layer beneath the PdAg surface alloy, the Ag surface atoms become less strongly bound to the underlying layer, so they interact more strongly with the adjacent Pd atoms of the surface alloy. This in turn reduces the interaction strength of the Pd surface atoms with adsorbates, which in our case is dominant for the H adsorption energy. This kind of ligand effect—the effect of neighboring Ag surface atoms—is missing for the $Pd_{1L}/Ag_{1L}/Pd_{3L}$ surface, which can at least partly explain the different effects of the Ag underlayer in the two systems.

3.2.4. Effect of Molecular H_2 Adsorption. So far we have calculated H adsorption energies for the adsorption of a single H atom. Experimentally, however, we expose the surface to a H_2 gas atmosphere. Since diffusion of H adatoms over pure Ag surface areas is strongly hindered (see the positive adsorption energy on an Ag surface layer presented in section 3.2.3), each Pd ensemble needs to accommodate an even number of H adatoms. To account for this effect, we calculated adsorption energies for the adsorption of 2 H atoms on a Pd_n ensemble, where the 2 H atoms arise from the dissociation of an impinging H_2 molecule. The calculated adsorption energies differ from the single atom adsorption energies due to (repulsive) interactions between neighboring H adatoms on these clusters. Dissociation pathways of the H_2 molecule are presented in detail and discussed in section 3.2.5.

Table 4 shows the effect of adsorbing 2 H atoms on the adsorption energy for dissociative H_2 adsorption for different

Table 4. Adsorption Energies of Two H Atoms on the PdAg/Pd(111) Surface Alloy Considering Various Ensemble Sizes[a]

	PBE/PAW		
	site	(3 × 3)	(5 × 5)
Pd_1	T	**−0.14**	
	fcc*/fcc*	−0.10	−0.14
Pd_2	T	−0.16	
	B/hcp*	−0.27	−0.25
	B/fcc*	**−0.28**	−0.26
	fcc*/fcc*	−0.18	−0.17
Pd_3-c	T	−0.17	
	fcc/fcc*	**−0.37**	−0.32
Pd_3-1	T	−0.16	
	B/B	**−0.44**	−0.38
Pd_3-b	T	−0.16	
	fcc*/fcc*	**−0.42**	−0.36
Fd_4	T	−0.18	
	fcc/fcc*	**−0.49**	−0.40
Pd_5	T	−0.17	
	fcc/fcc	**−0.60**	−0.49

[a] $Pd_{3\text{-}c}$, $Pd_{3\text{-}l}$, and $Pd_{3\text{-}b}$ denote the compact, linear, and bent Pd_3 ensembles. T, fcc, hcp, and B denote top, fcc-hollow, hcp-hollow, and bridge sites, respectively. Sites marked with an asterisk denote hollow positions around the ensemble. Bold values denote the preferential adsorption sites in each case (stable adsorption). Values are given in eV/atom, calculated using PBE/PAW and two different unit cells. Values for the T site correspond to the non-dissociated H_2 molecule (see text; calculated only for the 3 × 3 unit cell). For a visual description of the H_2 and 2H adsorption configurations, see Figure 7.

Pd_n ensembles and different configurations of the adsorbed H atoms. The different H_2 and 2H adsorption configurations are presented in Figure 7. Since several Pd ensembles like linear Pd_3 or compact Pd_5 ensembles would touch each other in neighboring unit (3 × 3), leading to an infinitely long string of connected ensembles, we also performed calculations using a (5 × 5) unit cell for the sake of comparison, in which these units are separated again by Ag surface atoms (see Figure 8). In general, adsorption energy values obtained using this larger unit cell are very close to those obtained for the (3 × 3) unit

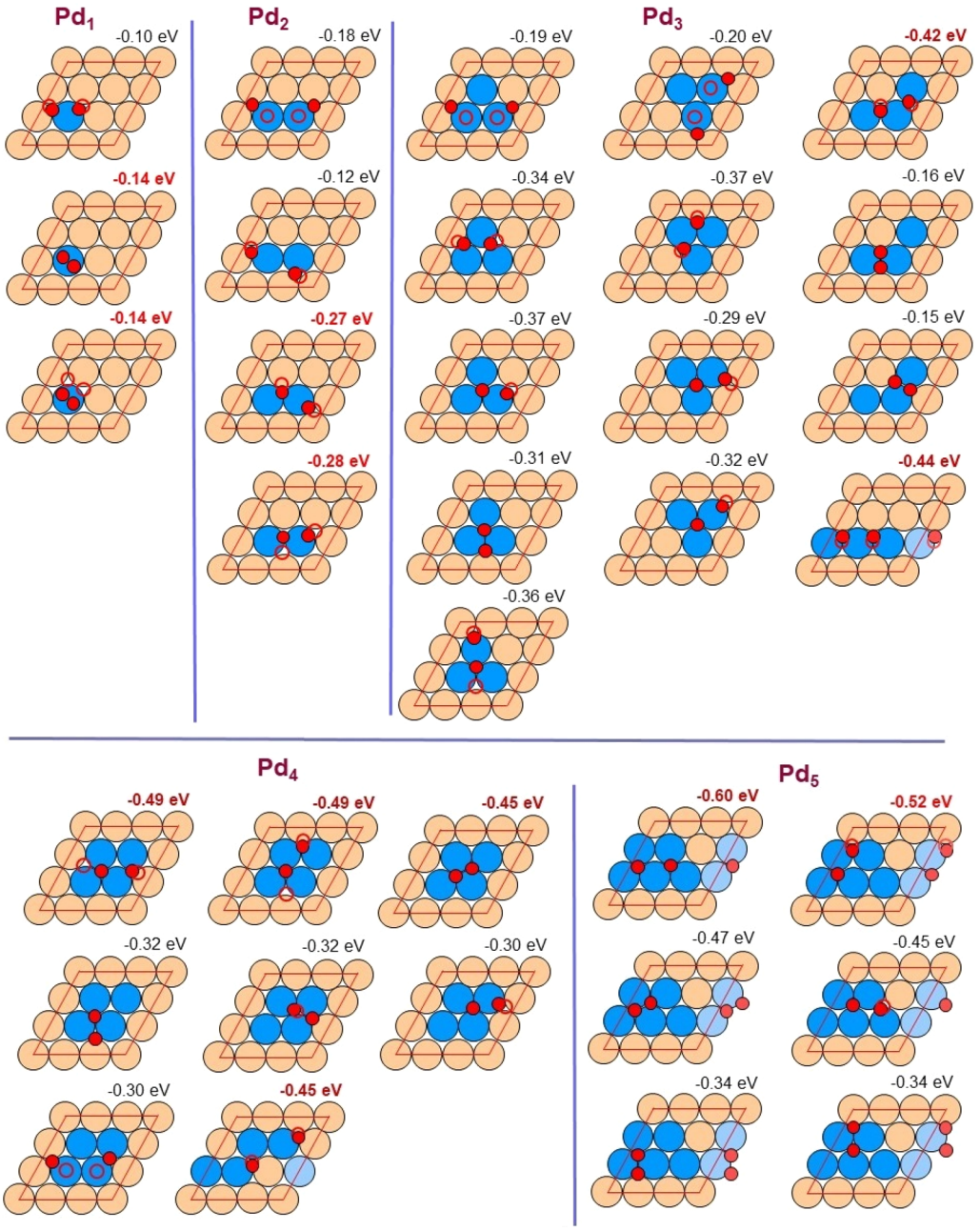

Figure 7. Adsorption of two H atoms on Pd_1, Pd_2, Pd_3, Pd_4, and Pd_5 ensembles of PdAg/Pd(111) surface alloys. Empty and filled red circles denote the initial and the final position of the H atoms, respectively. Bold red values highlight the largest adsorption energies in each case. Values are given in eV/adatom, calculated using PBE/PAW in a 3 × 3 unit cell. Due to the periodicity of the unit cell, a linear Pd_3 ensemble leads to an infinite linear chain, and the noncompact Pd_4 ensemble as well as the Pd_5 ensemble lead to infinite nonlinear chains of Pd atoms. In those cases, Pd and H atoms appearing due the periodicity are represented with lighter colors.

cell, though not exactly identical. The small differences arise from the different H and Pd concentrations obtained when increasing the size of the surface unit cell.

Starting with adsorption on a Pd_1 monomer, we note that if the two H atoms approach an isolated Pd_1 atom as a H_2 molecule from above, they become molecularly trapped. Such local minima for molecular H_2 adsorption are well-known for palladium surfaces.[69,70] However, for a Pd_1 monomer, the H_2 molecule does not dissociate due to its repulsive interactions with the neighboring Ag atoms. Only upon impinging on a Pd atom in larger Pd_n ensembles do they spontaneously dissociate (see the following section) upon adsorption at the top site, and the H adatoms would migrate to the nearest hollow sites. Stable molecular H_2 adsorption has in fact been experimentally observed and theoretically confirmed for hydrogen adsorption on the step sites of a Pd(210) surface,[69,70] if the further H_2 dissociation is hindered by the presence of coadsorbed hydrogen atoms. Therefore, the adsorption energies given in Table 4 for the top sites correspond to molecular H_2 adsorption, which were obtained by fixing the lateral x and y coordinates of the H atoms at the H−H distance corresponding to the well for the adsorbed H_2 molecule at the Pd_1 site (see Figure 7). The adsorption energies of H_2 on a top site of Pd_1, Pd_2, Pd_3, Pd_4, and Pd_5 are between −0.14 and −0.18 eV, well below the value needed to support adsorption at 100 K. In all situations, in the most stable configuration the

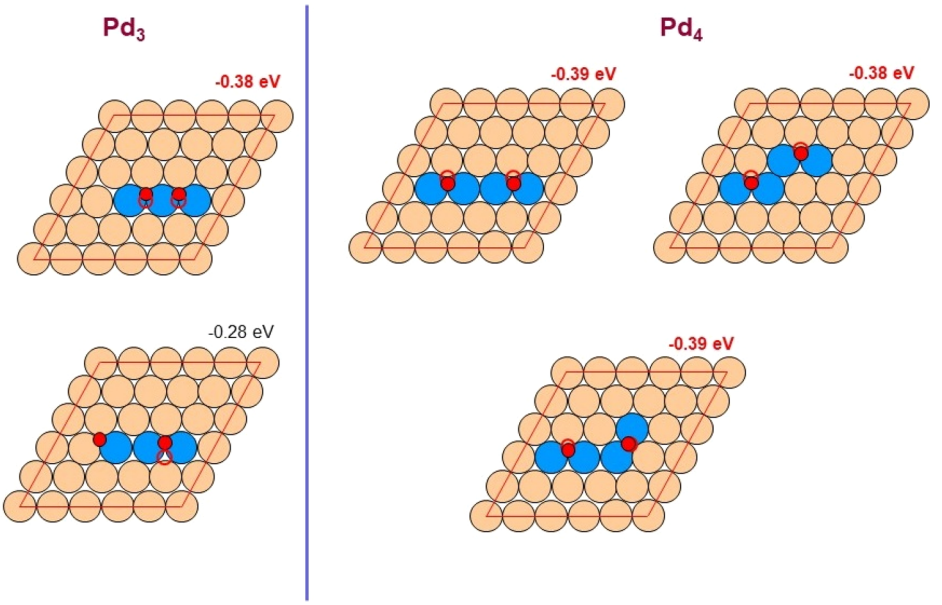

Figure 8. Adsorption of two H atoms on Pd_3 and Pd_4 ensembles of PdAg/Pd(111) surface alloys. Empty and filled red circles denote the initial and the final position of the H atoms, respectively. Values are given in eV/atom, calculated using PBE/PAW in a 5 × 5 unit cell.

H_2 molecular axis is parallel to the surface, whereas the adsorption energy for an upright H_2 molecule is almost zero.

Going to adsorption on Pd_2 ensembles, we find that the impinging H_2 molecule dissociates spontaneously (see section 3.2.5). If the two H atoms located at neighboring top sites of Pd_2 (one at each top site) are allowed to relax without coordinate constraints, then these repel each other along the axis of the ensemble toward the bridge sites at the ends with a small H adsorption energy of about −0.08 eV/atom. Further relaxation of this system brings the H atoms further apart to mixed Pd_1Ag_2 fcc-hollow sites at the ends of the ensemble, with a final adsorption energy of −0.18 eV/atom (Figure 7). The most stable, however, would be a configuration where one H adatom is located at the bridge site (tilted to H-fcc) and the other one at an fcc-hollow site at the end (slightly tilted to the top site) (adsorption energy −0.28 eV/atom). This latter configuration will not be reached spontaneously upon initial adsorption on the bridge sites, but it is easily accessible via thermal activation at the experimental adsorption temperature of 80 K.

A similar behavior is observed if two H atoms are initially located at neighboring top sites of $Pd_{3\ c}$. The energetics of this relaxation pathway are illustrated in Figure 9. In the final configuration arising from this initial adsorption site, the H adatoms are located at asymmetric, mixed Pd_1Ag_2 fcc-hollow sites, with an adsorption energy of −0.19 eV/atom. More stable adsorption, however, is reached for other initial and relaxed configurations (see Figure 7). The lowest adsorption energy for adsorption of two H atoms on a compact $Pd_{3\ c}$ ensemble is −0.37 eV/atom, with one H atom at the inner fcc-hollow site and the other at one of the closer fcc-hollow sites around the ensemble. Also in this case, we expect that even at 100 K thermal activation would be sufficient to reach this stable configuration when starting from other adsorption configurations. The trend in the adsorption energies derived from Figure 7 further indicates that the particular configuration of the adsorption site is highly critical, with adsorption on a fcc-hollow Pd_3 site being most favorable, but for adsorption at very close distances, e.g., on two directly neighboring 3-fold

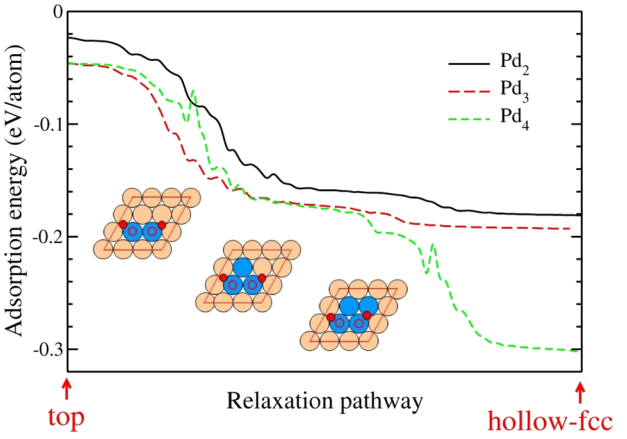

Figure 9. Adsorption energy of two individual H atoms arising from the dissociative adsorption of a H_2 molecule on neighboring top sites along the relaxation pathway from top sites to outer fcc-hollow sites of a Pd_n ensemble in a PdAg/Pd(111) surface alloy, calculated using a 3 × 3 unit cell and an H_{ad} coverage of $^2/_9$. Energy is given in eV/atom. Empty and filled red circles denote the initial and the final position of the H atoms, respectively. The small peaks are most likely due to numerical noise of the minimization algorithm used in the DFT code; thus, they do not describe a real energy barrier.

hollow sites, H_{ad}–H_{ad} repulsions are sufficiently strong to preclude them as stable adsorption sites.

For a Pd_3 linear ensemble, which corresponds to a linear chain in a 3 × 3 unit cell, the strongest adsorption of two H atoms (−0.44 eV/atom) occurs when these atoms are located at the bridge sites. Similarly to Pd_2, the H atoms are slightly displaced toward the fcc-hollow sites (asymmetric Pd_2Ag_1 hollow sites). Calculations for H adsorption in a 5 × 5 unit cell, where these ensembles are separated and do not form a continuous string of atoms, result in a very similar adsorption energy of −0.38 eV/atom, and this is also the most stable adsorption configuration. For a bent Pd_3 trimer, adsorption on neighboring asymmetric Pd_2Ag_1 fcc-hollow sites was found to be most stable, while configurations with one H adatom

occupying a Pd_2Ag_1 fcc-hollow and the other at the closest Pd_2Ag_1 hcp-hollow site were less stable, reflecting the influence of H_{ad}−H_{ad} repulsions and the preference for fcc-hollow sites.

A similar behavior is observed if two H atoms are located at neighboring top sites of a compact $Pd_{4\ c}$ tetramer. In that case, the final adsorption energies can vary depending on which top sites are involved in the initial adsorption. The highest binding energy of two H atoms (−0.49 eV/atom) is obtained when these are located at adjacent fcc-hollow sites, one at the inner part, a Pd_3 ensemble, and the other one around the ensemble (mixed Pd_2Ag_1 ensemble). Due to H_{ad}−H_{ad} repulsion and the site preference for fcc-hollow sites this configuration is more stable than the one with both H adatoms located in directly neighboring Pd_3 sites, one fcc-hollow and the other one a hcp-hollow site. For bent and linear Pd_4 ensembles the situation is similar to that in bent and linear Pd_3 ensembles.

Finally, for a compact Pd_5 ensemble, the situation is comparable to that in Pd_4. In this case, however, it is possible to occupy two neighboring fcc-hollow sites on Pd_3-type ensemble in the inner part of the ensemble. This results in an increase of the adsorption energy to −0.60 eV/atom, which is essentially identical to that on Pd(111) at comparable local H_{ad} coverage. Hence, Pd_5 would be the first ensemble to behave similar to the Pd(111) surface when the H coverage increases (see Table 1). Calculations for H adsorption in a 5 × 5 unit cell, where these Pd_5 ensembles are separated from each other, led to the same trends in the values as for the 3 × 3 unit cell, although with slightly higher energies (by ∼0.1 eV/atom, due to the different H coverage).

Overall, these calculations lead to the following conclusions: As expected from the adsorption behavior of single H atoms, occupation of Pd_3 sites is more favorable than that of Pd_2Ag_1 or even Pd_1Ag_2 sites, which leads to a significant stabilization of the H_{ad} species on the $Pd_{4\ c}$ ensemble as compared to Pd_2 and $Pd_{3\ c}$ ensembles. Furthermore, adsorption on fcc-hollow sites is generally favored compared to that on hcp-hollow sites or on mixed sites. Occupation of the nearest neighbor hollow sites is generally less favorable, due both to repulsive H_{ad}−H_{ad} interactions and because of the preference for fcc-hollow sites. For adsorption on $Pd_{4\ c}$ tetramers, this means that adsorption of the first H adatom on a Pd_3 site and of the second H adatom on a Pd_2Ag_1 site at the side of the tetramer is more stable than adsorption of both adatoms on nearest neighbor Pd_3 sites. This also means that the compact $Pd_{5\ c}$ pentamer is the smallest ensemble allowing H_2 dissociative adsorption with an adsorption energy comparable to that of Pd(111).

Finally, adsorption of three or more H atoms per ensemble was tested only for some particular cases, due to the immense number of possible configurations. In general, the adsorption energy per atom decreases as the number of H atoms increases, both due to H_{ad}−H_{ad} repulsion and due to the occupation of less strongly binding adsorption sites, but there is no unique pattern to correlate the number of H adatoms adsorbed with the adsorption energy.

3.2.5. H_2 Dissociation. Dissociation of the H_2 molecule was investigated using the nudged elastic band (NEB) method[55,56] by following the energetic evolution of the molecule from a position sufficiently far away from the alloy surface toward the most favorable position for adsorption of the two individual atoms on the respective Pd_n ensemble. The initial position of the H_2 molecule was set to ∼3.5 Å above the surface alloy at the center of each palladium ensemble and oriented parallel to the surface. We assumed the bond length of the free molecule was the experimental one, 0.74 Å.[71] As shown in section 3.2.4, the minimum energy configuration for adsorption of two H atoms on a Pd_1 monomer is the H_2 molecule on the top site (−0.14 eV/atom). In contrast, larger palladium ensembles allow dissociation of H_2 molecules, starting with preliminary adsorption of the molecule on a top site, followed by bond splitting to reach a minimum energy configuration. In most of these final configurations, the individual H atoms are adsorbed on two hollow sites of each of the palladium ensemble. The adsorption energies of 2 H atoms along the relaxation pathway from the gas phase (as a H_2 molecule) to the minimum energy configuration with two individual H atoms adsorbed on a Pd_n ensemble in a PdAg/Pd(111) surface alloy are illustrated in Figure 10, which shows NEB results for Pd-induced

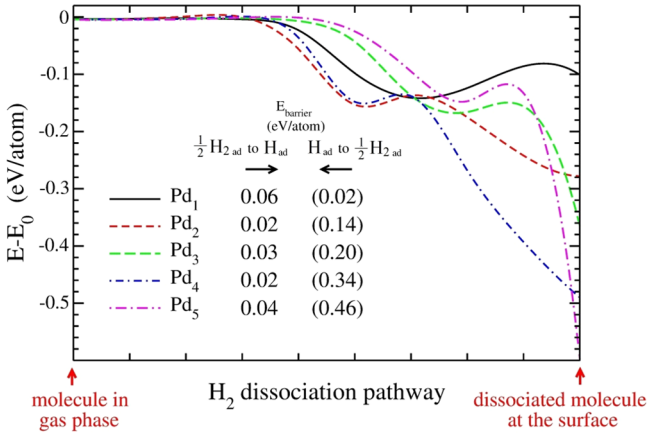

Figure 10. Adsorption energy of two H atoms along the minimum energy pathway for H_2 dissociation from the gas phase (as a H_2 molecule) to the minimum energy configuration for two individual H atoms adsorbed on a Pd_n ensemble in a PdAg/Pd(111) surface alloy, where both atoms are allowed to relax freely while approaching the surface. Energies (given in eV/atom) were calculated within a 3 × 3 unit cell using the NEB method. For each Pd ensemble size, we report the energy barrier for dissociation and the energy barrier for the inverse process (in parentheses). For Pd_1, the path ends at the local minimum, while for the other ensembles it ends at the global minimum.

dissociation of the H_2 molecule on Pd_1−Pd_5 ensembles. Energies (in eV/atom) were calculated within a 3 × 3 unit cell. For each Pd_n ensemble size, we report the energy barrier for dissociation from the molecular precursor state and the energy barrier for the inverse recombination process (in parentheses). For Pd_1, the path ends at the local minimum (molecular adsorption), while for the other ensembles, it ends at the global minimum (dissociative adsorption). Although the most stable configuration for two H atoms on Pd_1 is the adsorbed molecule at the top site, we extend its NEB path up to the only local minimum in which the H atoms are dissociated.

Figure 10 clearly demonstrates that there is an energy minimum for molecular H_2 adsorption with similar energies for all ensemble sizes between −0.14 and −0.17 eV/atom. For the Pd_1 monomer, the energy barrier to dissociate the H_2 molecule adsorbed on top of the Pd atom toward the surrounding hollow sites is 0.06 eV, which is less than the barrier for desorption of $H_{2,ad}$. Considering that $H_{2,ad}$ is energetically more favorable than two H_{ad} on this site, this means that at very low temperatures it should be possible to stabilize molecularly adsorbed H_2 on these sites. Under our

experimental conditions, however, at 80−90 K, this does not play a role. In total, these results clearly demonstrate the facile dissociation of adsorbing H_2 molecules on all ensembles and sites except for the on-top site on Pd_1 monomers.

4. DISCUSSION

On the basis of the DFT calculations presented in the previous section and of the ensemble statistics derived previously from an STM-based analysis of the surface atom distribution as a function of Pd surface concentration,[41] we will now discuss the peaks observed in the TPD spectra shown in section 3.1.2 and their physical origin. Here it is important to note that diffusion of H_{ad} species over Ag surface areas is essentially inhibited, as the barrier for entering these areas is comparable to or even larger than that for desorption. This is illustrated by the simultaneous filling of the different peaks with increasing D_2 exposure (Figure 3). Otherwise, we would expect the most stable sites to be populated first, followed by the less stable ones. Hence, we can concentrate on the adsorption behavior of an even number of H atoms on the individual Pd ensembles, where the H atoms result from the dissociative adsorption of H_2 molecules. For the smaller Pd_n ensembles ($n \leq 4$), which are dominant at lower Pd surface concentrations, this essentially means two H adatoms per ensemble. Furthermore, we assume that even at the low adsorption temperature of 80−90 K diffusion of H adatoms to the most stable adsorption configuration is facile because of low diffusion barriers. Finally, we can use the main result of the STM-based analysis of the surface distribution in the PdAg/Pd(111) surface alloys, which revealed a nearly random distribution of the two metals in the surface layer for the whole range of surface compositions.[41]

First, based on the very low H_2 adsorption energy on a Pd_1 ensemble, we can exclude stable H adsorption on these sites at the adsorption temperatures of ≥80 K in our experiments. Larger Pd ensembles, starting from Pd_2, instead allow H_2 dissociation. The most favorable configuration of two H atoms on an isolated Pd_2 ensemble yields an adsorption energy of ∼0.28 eV/atom, i.e., ∼0.56 eV/H_2 molecule, which would fit to the activation energy for desorption of 0.4 eV estimated for the γ_1 peak. Here we assume nonactivated adsorption, so the adsorption energy and activation energy for desorption are approximately identical. From the surfaces whose D_2-TPD spectra are shown in Figure 1, the surface alloys with 5 and 8% Pd should feature ∼0.2 and ∼0.5−1% of the surface atoms, respectively, as Pd_2 ensembles, while larger Pd ensembles are not very likely for these surfaces. Obviously, for the first surface (5% Pd) the number of Pd_2 ensembles is too low to result in a clear D_2-TPD peak above the background desorption signal. For the second surface (8% Pd), however, a weak γ_1 peak can be observed and its intensity (0.01 ML after background subtraction) fits rather well to the expected number of isolated Pd_2 ensembles. Going to higher Pd surface concentrations, this peak increases in intensity up to about 50% Pd surface content, and then decreases rapidly. On the basis of the STM results, the number of isolated Pd_2 sites should, after an initial increase, decay quickly with increasing Pd content and finally tend to almost zero for the surfaces with the highest Pd concentration. Here we need to keep in mind, however, that sites with comparable adsorption energies may exist also at larger ensembles for higher local coverages, which would shift the maximum population of this peak to higher Pd concentrations, in good agreement with experimental observation.

On the basis of the adsorption energies, the γ_2 peak with its slightly higher adsorption energy compared to the γ_1 state can then be assigned to desorption from Pd_3 and Pd_4 ensembles. Calculations for the most stable adsorption configuration on Pd_3 ensembles of different shape yielded maximum adsorption energies between −0.37 and −0.44 eV/atom, while for Pd_4 the maximum adsorption energy was −0.49 eV/atom, still close to those of the various Pd_3 ensembles. This would explain why the γ_2 peak shows a main peak (at ∼195 K) and a shoulder at ∼170 K. According to the STM results,[41] a surface with 26% Pd, which is where the γ_2 peak appears first, shows not only a substantial number of Pd_2 sites (∼7%), but also some larger ensembles. In fact, the number of Pd_3 ensembles is with ∼2% of all sites also sizable, fitting well to the appearance of the γ_2 peak with a single peak at ∼170 K for this surface. Also the integrated D_{ad} coverage of the two γ features in the D_2-TPD spectrum of this surface of ∼5% compares favorably with the concentrations in the STM images.

Desorption from isolated Pd_4 ensembles should also play a role since adsorption of two H atoms on them yields adsorption energies close to those of the trimers (see Table 4). The assignment of the γ_2 feature to desorption from Pd_3 and Pd_4 ensembles becomes more reasonable when looking at the spectrum of the surface with 49% Pd in Figure 1. The γ_2 feature shows a main peak (at ∼195 K) and a shoulder (at ∼170 K), where the former is attributed to desorption from Pd_4 ensembles. With increasing Pd surface content, this peak also disappears quickly, reflecting the disappearance of isolated $Pd_{3\,c}$ and $Pd_{4\,c}$ clusters with increasing Pd concentration.

The dissociative adsorption energy for two H atoms at Pd_5 reaches −0.60 eV/atom. This is larger than for the smaller ensembles and close to the adsorption energy of an isolated H atom at the fcc-hollow site of the Pd(111) surface (see Table 1). Hence, this would perfectly fit to the pronounced β peak, which appears at intermediate Pd surface concentrations (≥33%) and then rapidly increases with increasing Pd surface concentration. Indeed, the STM data show that Pd_5 ensembles appear with very low concentrations in this coverage range. With increasing Pd coverage, these and larger Pd ensembles increasingly dominate the site distribution. A small shift of the β peak to higher temperatures with increasing Pd surface content may be related to an increasing content of slightly more stable sites for larger Pd_n ensembles with $n > 5$.

In total, on the basis of the combination of STM-based site analysis and DFT calculated adsorption energies, we could provide a consistent explanation for the physical origin of the different desorption peaks, both with respect to the adsorption energy and with respect to their relative population with increasing Pd surface concentration.

Finally, we compare our results with the findings of a similar study of H adsorption on PdAu/Pd(111) surface alloys,[46,47] a seemingly very similar bimetallic system in which also a noble metal is mixed into the surface layer of the Pd(111) crystal. The structural properties are very similar for both systems, as PdAu/Pd(111) surface alloys show also a random distribution of the respective atoms in the surface layer for the complete range of surface compositions.[47] Some dissolution of the noble metal upon annealing for surface alloy formation is also encountered for PdAu/Pd(111) after depositing larger Au amounts close to a monolayer. Therefore, noble metal atoms in the second or deeper layers may affect H adsorption in both type of alloys in a rather similar way, mainly at high Ag or Au coverages. Furthermore, H adsorbates are confined to the Pd_n

ensembles when H_2 molecules reach the surface of Au-rich PdAu/Pd(111) surface alloys, i.e., diffusion of H adatoms above Au surface regions between isolated Pd_n ensembles is also unlikely, allowing stable adsorption on a Pd_n ensemble only if this can accommodate both H adatoms resulting from dissociative H_2 adsorption. Despite these similarities, there are some interesting differences in the H_2 adsorption behavior of these two systems. While we conclude for PdAg/Pd(111) that a Pd_2 ensemble should be sufficient to achieve stable adsorption of two H adatoms under our experimental conditions, Takehiro et al.[47] arrived at a different result for hydrogen adsorption on PdAu/Pd(111) surfaces alloys. They concluded that a Pd_4 rhombic ensemble is the minimum ensemble size required for stable adsorption of two H adatoms on PdAu/Pd(111) surfaces. This discrepancy can be explained in part by the different starting temperature for hydrogen exposure, 90 K for PdAg/Pd(111) versus 120 K for PdAu/Pd(111). Most strikingly, the γ_1 peak would not be populated anymore at 120 K. Furthermore, DFT calculations also revealed some characteristic differences in the local reactivity of these surface alloys. To exclude contributions from systematic differences between these calculations, we additionally calculated the adsorption energy of two hydrogen atoms at the linear Pd_3 ensemble in the PdAu/Pd(111) surface alloy. While the binding strength is −0.44 eV/atom when the ensemble is surrounded by Ag atoms, it is significantly lower (−0.29 eV) when it is instead surrounded by Au atoms. Also assuming a similar trend for compact $Pd_{3\,c}$ ensembles, this implies that H_2 desorption from Pd_3 ensembles in PdAu/Pd(111) surfaces might occur at lower temperatures than for PdAg/Pd(111) surfaces, presumably below the adsorption temperature of 120 K in these experiments; therefore, these ensembles cannot contribute to adsorption under those conditions. This could explain why the desorption features for H_2 on PdAu/Pd(111) surfaces observed by Takehiro et al.[47] were assigned only to Pd ensembles starting with Pd_4.

Comparing adsorption of H_2 on these bimetallic PdAg surfaces with that of CO on the same surfaces,[42,43,64] there are many similarities in the trends of the adsorption energies on different Pd_n ensembles and sites. This fully agrees with expectations based on the d-band model[72] since in both cases the changes in the adsorption energy should be correlated with the respected shifts in the center of the d-band. Interestingly, however, for both CO and H adsorption, the (calculated) adsorption energy on Pd_n ensembles decreases in the presence of a Ag underlayer, despite of the simultaneous upshift of the center of the d-band. However, there are also distinct differences. First, the relative differences in the adsorption energies on different Pd_n ensembles and sites are much less pronounced for CO than for H adsorption. In particular, the preference for adsorption on 3-fold hollow sites is less pronounced. Second, considering that adsorption energies are generally larger for CO adsorption this also means that essentially all ensembles can be populated during adsorption at 80−90 K, which is in distinct contrast to H adsorption, where Pd_2 dimers are the smallest ensembles supporting stable H adsorption under these conditions. Third, CO molecules impinging on Ag surface areas in the neighborhood of Pd_n ensembles can reach these Pd sites, which makes the effect of the Pd surface concentration on the measured CO uptake much less significant than for H_2 adsorption. Because of the small differences in CO adsorption energies on different sites, we could not decide whether CO_{ad} transport between different Pd_n ensembles is possible or whether it can be excluded as in the case of hydrogen adsorption.

Finally, we would like to comment on possible consequences of these results on catalytic hydrogenation reactions. While it is hardly possible to create and maintain surface alloys of the present type, with Ag or Au atoms only in the topmost layer, in realistic catalysts, we assume that the random distribution of surface atoms is likely to be maintained also in bulk alloys. In that case, these bimetallic surfaces can provide a whole arsenal of adsorption sites of different adsorption strength. Considering that based on the Sabatier principle the adsorption strength is often closely linked to the catalytic activity and possibly also to the selectivity of these sites, this allows us to finely tune the reactivity of these (surface) alloys in a given reaction by optimizing the (surface) concentration of Pd, in good agreement with experimental findings for either of these alloys, e.g., in hydrogenation reactions for PdAg[10−13] or in vinyl acetate synthesis or H_2O_2 formation on supported PdAu catalysts.[73−77] In that sense, the present data should be considered as a means to provide a picture of the reactivity of these surfaces at a given surface composition; the preparation of such kind of bimetallic catalyst surfaces and maintaining them under reaction conditions, which can lead to changes in the surface composition,[10,21,22] have to be considered separately.

5. CONCLUSIONS

We have investigated the adsorption of hydrogen on structurally well-defined PdAg/Pd(111) surface alloys by a combination of DFT calculations and TPD measurements, in combination with previous results of high-resolution STM measurements. Comparing the calculated adsorption energies on different adsorption sites and different Pd_n ensembles, the abundance of these sites/ensembles at given Pd surface concentrations (STM analysis) and the evolution of the TPD spectra with increasing Pd surface concentration, we could correlate the different peaks in the TPD spectra and their activation energy for desorption with specific adsorption sites on the surface, i.e., well-defined Pd ensembles. We assign the γ_1 peak (at ∼120 K) to desorption from Pd_2 ensembles, the γ_2 peak at ∼195 K with a shoulder at ∼170 K to desorption from Pd_4 and Pd_3 ensembles, respectively, and the β peak (at ∼310 K) to desorption from Pd_5 and larger ensembles. In all cases, adsorption of individual H atoms on Pd_3-type hollow sites is most stable, followed by adsorption on asymmetric Pd_2Ag_1-type and finally Pd_1Ag_2-type hollow sites. Furthermore, H adsorption is always more stable on fcc-type sites than on hcp-type sites. Generally, the trends agree with those for CO adsorption and shifts in the d-band center reported earlier.[64] Initially, the adsorption behavior is affected by the fact that transport of H_{ad} between isolated Pd_n ensembles, which are separated by Ag surface areas, is kinetically hindered, meaning that the uptake of H adatoms on a given Pd_n ensemble is possible only pairwise, to accommodate the two H_{ad} atoms arising from adsorption of one H_2 molecule.

On the basis of the DFT calculations, H_2 dissociation is unfavorable for adsorption on a Pd_1 monomer, favoring molecular hydrogen adsorption on these sites. The resulting adsorption energy is, however, too low to stabilize H_2 adsorption at temperatures >80 K. In case of larger ensembles, we predict dissociative hydrogen adsorption, with metastable molecular adsorption at top sites as intermediate, followed by

an activation energy of less than 0.04 eV, leading to the final stable adsorption site.

Pd_2 ensembles are identified as the minimum ensemble size allowing adsorption on PdAg/Pd(111) surface alloys under our experimental conditions. The difference from the earlier report of a comparable study on PdAu/Pd(111) surface alloys,[47] where Pd_4 tetramers were concluded as minimum ensemble size, most probably results from a combination of somewhat lower adsorption energies on the latter surfaces, reflecting characteristic differences in the way Ag and Au ligands influence the reactivity of the Pd surface atoms, and a higher adsorption temperature (120 K) in the latter experiments. On a qualitative scale, these trends can be fully reconciled by a combination of electronic ligand effects, geometric ensemble effects and strain effects, together with bond order arguments.

Overall, this type of model studies provides detailed insights into the chemical and thus also catalytic behavior of bimetallic surfaces and catalysts which is highly useful also for the mechanistic understanding of reactions on bimetallic catalysts, in this case on supported PdAg catalysts. Due to the wide variation in adsorption energies on these bimetallic surface, they allow a precise tuning of the adsorption energy and thus of the activity in catalytic reactions by adjusting the Pd surface content.

AUTHOR INFORMATION

Corresponding Author

R. Jürgen Behm − *Institute of Surface Chemistry and Catalysis, Ulm University, D-89081 Ulm, Germany;* Present Address: Institute of Theoretical Chemistry, Ulm University, Albert-Einstein-Allee 11, D-89081 Ulm, Germany; orcid.org/0000-0002-7565-0628; Email: juergen.behm@uni-ulm.de

Authors

Luis A. Mancera − *Institute of Theoretical Chemistry, Ulm University, D-89081 Ulm, Germany*

Thomas Diemant − *Institute of Surface Chemistry and Catalysis, Ulm University, D-89081 Ulm, Germany;* Present Address: Helmholtz Institute Ulm Electrochemical Energy Storage (HIU), Helmholtzstr. 11, D-89081 Ulm, Germany

Axel Groß − *Institute of Theoretical Chemistry, Ulm University, D-89081 Ulm, Germany;* orcid.org/0000-0003-4037-7331

Complete contact information is available at: https://pubs.acs.org/10.1021/acs.jpcc.1c10070

Notes

The authors declare no competing financial interest.

ACKNOWLEDGMENTS

This study was supported by the German Science Foundation (DFG) via the Research Unit 1376 (contract Be 1201/18-1) and by the Baden-Württemberg Foundation via the project CT-4 "ORR-Scale" within the program "Clean Tech". Computational resources were provided by the JUSTUS high-performance computing facility at Ulm University as part of the bwHPC-C5 initiative of the federal state of Baden-Württemberg and the German Research Foundation (DFG) through Grant INST 40/467-1 FUGG.

REFERENCES

(1) Ponec, V. Alloy Catalysts: the Concept. *Appl. Catal., A* **2001**, *222*, 31−45.

(2) Sinfelt, J. H. Role of Surface Science in Catalysis. *Surf. Sci.* **2002**, *500*, 923−946.

(3) Ponec, V.; Sachtler, W. M. H. The Reactions Between Cyclopentane and Deuterium on Nickel and Nickel-Copper Alloys. *J. Catal.* **1972**, *24*, 250−261.

(4) Sinfelt, J. H.; Carter, J. L.; Yates, D. J. C. Catalytic Hydrogenolysis and Dehydrogenation Over Copper-Nickel Alloys. *J. Catal.* **1972**, *24*, 283−296.

(5) Sachtler, W. M. H. Surface Composition of Alloys in Equilibrium. *Le Vide* **1973**, *164*, 67−71.

(6) Soma-Noto, Y.; Sachtler, W. M. H. Infrared Spectra of Carbon Monoxide Adsorbed on Silica-Supported Nickel-Copper Alloys. *J. Catal.* **1974**, *34*, 162−164.

(7) Mavrikakis, M.; Hammer, B.; Nørskov, J. K. Effect of Strain on the Reactivity of Metal Surfaces. *Phys. Rev. Lett.* **1998**, *81*, 2819−2822.

(8) Groß, A. Reactivity of Bimetallic Systems Studied From First Principles. *Top. Catal.* **2006**, *37*, 29−40.

(9) Groß, A. Tailoring the Reactivity of Bimetallic Overlayer and Surface Alloy Systems. *J. Phys.: Condens. Matter* **2009**, *21*, 084205.

(10) Jin, Y.; Datye, A. K.; Rightor, E.; Gulotty, R. T.; Waterman, W.; Smith, M.; Holbrook, M.; Maj, J.; Blackson, J. The Influence of Catalyst Restructuring on the Selective Hydrogenation of Acetylene to Ethylene. *J. Catal.* **2001**, *203*, 292−306.

(11) Zhang, Q.; Li, J.; Liu, X.; Zhu, Q. Synergetic Effect of Pd and Ag Dispersed on Al_2O_3 in the Selective Hydrogenation of Acetylene. *Appl. Catal., A* **2000**, *197*, 221−228.

(12) Zea, H.; Lester, K.; Datye, A. K.; Rightor, E.; Gulotty, R.; Waterman, W.; Smith, M. The Influence of Pd-Ag Catalyst Restructuring on the Activation Energy for Ethylene Hydrogenation in Ethylene-Acetylene Mixtures. *Appl. Catal., A* **2005**, *282*, 237−245.

(13) Luneau, M.; Lim, J. S.; Patel, D. A.; Sykes, E. C.; Friend, C. M.; Sautet, P. Guidelines to Achieving High Selectivity for the Hydrogenation of v-Unsaturated Aldehydes With Bimetallic and Dilute Alloy Catalysts: A Review. *Chem. Rev.* **2020**, *120*, 12834−12872.

(14) Beckord, S.; Brimaud, S.; Behm, R. J. Stability and ORR Performance of a Well-Defined Bimetallic $Ag_{70}Pt_{30}$/Pt(111) Monolayer Surface Alloy Electrode - Probing the De-Alloying at an Atomic Scale. *Electrochim. Acta* **2018**, *259*, 762−771.

(15) Beckord, S.; Brimaud, S.; Behm, R. J. The Performance of Structurally Well-Defined Ag_xPt_{1-x}/Pt(111) Surface Alloys in the Oxygen Reduction Reaction-An Atomic-Scale Picture. *J. Electroanal. Chem.* **2018**, *819*, 401−409.

(16) Zamora-Zeledón, J. A.; Stevens, M. B.; Gunasooriya, G. T. K.; Gallo, A.; Landers, A. T.; Kreider, M. E.; Hahn, C.; Nørskov, J. K.; Jaramillo, T. F. Tuning the Electronic Structure of Ag-Pd Alloys to Enhance Performance for Alkaline Oxygen Reduction. *Nat. Commun.* **2021**, *12*, 620.

(17) Shu, J.; Grandjean, B. P. A.; Van Neste, A.; Kaliaguine, S. Catalytic Palladium-Based Membrane Reactors: A Review. *Can. J. Chem. Eng.* **1991**, *69*, 1036−1060.

(18) Svenum, I. H.; Herron, J. A.; Mavrikakis, M.; Venvik, H. J. $Pd_3Ag(111)$ As a Model System for Hydrogen Separation Membranes: Combined Effects of CO Adsorption and Surface Termination on the Activation of Molecular Hydrogen. *Top. Catal.* **2020**, *63*, 750−761.

(19) Wouda, P. T.; Schmid, M.; Nieuwenhuys, B. E.; Varga, P. STM Study of the (111) and (100) Surfaces of PdAg. *Surf. Sci.* **1998**, *417*, 292−300.

(20) Walle, L. E.; Grönbeck, H.; Fernandes, V. R.; Blomberg, S.; Farstad, M. H.; Schulte, K.; Gustafson, J.; Andersen, J. N.; Lundgren, E.; Borg, A. Surface Composition of Clean and Oxidized $Pd_{75}Ag_{25}(100)$ From Photoelectron Spectroscopy and Density Functional Theory Calculations. *Surf. Sci.* **2012**, *606*, 1777−1782.

(21) van Spronsen, M. A.; Daunmu, K.; O'Connor, C. R.; Egle, T.; Kersell, H.; Oliver-Meseguer, J.; Salmeron, M. B.; Madix, R. J.; Sautet,

P.; Friend, C. M. Dynamics of Aurface Alloys: Rearrangement of Pd/Ag(111) Induced by CO and O_2. *J. Phys. Chem. C* **2019**, *123*, 8312−8323.
(22) Egle, T.; O'Connor, C. R.; Friend, C. M. Regeneration of Active Surface Alloys During Cyclic Oxidation and Reduction: Oxidation of H_2 on Pd/Ag(111). *J. Phys. Chem. Lett.* **2021**, *12*, 6752−6759.
(23) Kok, G. A.; Noordermeer, A.; Nieuwenhuys, B. E. Effects of Alloying on the Adsorption of CO on Palladium: a Comparison of the Behaviour of PdAg(111), PdCu(111) and Pd(111) Surface. *Surf. Sci.* **1985**, *152−153*, 505−512.
(24) Wouda, P. T.; Schmid, M.; Nieuwenhuys, B. E.; Varga, P. Adsorbate Migration on PdAg(111). *Surf. Sci.* **1999**, *423*, L229−L235.
(25) Conrad, H.; Ertl, G.; Latta, E. E. Adsorption of Hydrogen on Palladium Single Crystal Surfaces. *Surf. Sci.* **1974**, *41*, 435−446.
(26) Behm, R. J.; Christmann, K.; Ertl, G. Adsorption of Hydrogen on Pd(100). *Surf. Sci.* **1980**, *99*, 320−340.
(27) Cattania, M. G.; Penka, V.; Behm, R. J.; Christmann, K.; Ertl, G. Interaction of Hydrogen With a Palladium(110) Surface. *Surf. Sci.* **1983**, *126*, 382−391.
(28) Eberhardt, W.; Louie, S. G.; Plummer, E. W. Interaction of Hydrogen With a Pd(111) Surface. *Phys. Rev. B* **1983**, *28*, 465−477.
(29) Gdowski, G. E.; Felter, T. E.; Stulen, R. H. Effect of Surface Temperature on the Sorption of. Hydrogen by Pd(111). *Surf. Sci.* **1987**, *181*, L147−L155.
(30) Gdowski, G. E.; Stulen, R. H.; Felter, T. E. Summary Abstract: Isotopic Differences in Low-Temperature Sorption and Desorption of Hydrogen by Pd(111). *J. Vac. Sci. Technol. A* **1987**, *5*, 1103−1104.
(31) Groß, A.; Wilke, S.; Scheffler, M. Six-Dimensional Quantum Dynamics of Adsorption and Desorption of H_2 at Pd(100): No Need for a Molecular Precursor Adsorption State. *Surf. Sci.* **1996**, *357−358*, 614−618.
(32) Dong, W.; Ledentu, V.; Sautet, P.; Eichler, A.; Hafner, J. Hydrogen Adsorption on Palladium: a Comparative Theoretical Study of Different Surfaces. *Surf. Sci.* **1998**, *411*, 123−136.
(33) Pallassana, V.; Neurock, M.; Hansen, L. B.; Hammer, B.; Nørskov, J. K. Theoretical Analysis of Hydrogen Chemisorption on Pd(111), Re(0001) and Pd_{ML}/Re(0001), Re_{ML}/Pd(111) Pseudomorphic Overlayers. *Phys. Rev. B* **1999**, *60*, 6146−6154.
(34) Mitsui, T.; Rose, M. K.; Fomin, E.; Ogletree, D. F.; Salmeron, M. Dissociative Hydrogen Adsorption on Palladium Requires Aggregates of Three or More Vacancies. *Nature* **2003**, *422*, 705−707.
(35) Mitsui, T.; Rose, M. K.; Fomin, E.; Ogletree, D. F.; Salmeron, M. Hydrogen Adsorption and Diffusion on Pd(1 1 1). *Surf. Sci.* **2003**, *540*, 5−11.
(36) Lopez, N.; Lodziana, Z.; Illas, F.; Salmeron, M. When Langmuir Is Too Simple: H_2 Dissociation on Pd(111) at High Coverage. *Phys. Rev. Lett.* **2004**, *93*, 146103.
(37) Groß, A. Ab Initio Molecular Dynamics Simulations of the Adsorption of H_2 on Palladium Surfaces. *ChemPhysChem* **2010**, *11*, 1374−1381.
(38) Xu, L. S.; Ma, Y. S.; Zhang, Y. L.; Teng, B. T.; Jiang, Z. Q.; Huang, W. X. Revisiting H/Pt(111) by a Combined Experimental Study of the H-D Exchange Reaction and First-Principles Calculations. *Sci. China Chem.* **2011**, *54*, 745−755.
(39) Brimaud, S.; Engstfeld, A. K.; Alves, O. B.; Hoster, H. E.; Behm, R. J. Oxygen Reduction on Structurally Well-Defined, Bimetallic PtRu Surfaces: Monolayer Pt_xRu_{11x}/Ru(0001) Durface Alloys Versus Pt Film Covered Ru(0001). *Top. Catal.* **2014**, *57*, 222−235.
(40) Brimaud, S.; Engstfeld, A. K.; Alves, O. B.; Behm, R. J. Structure-Reactivity Correlation in the Oxygen Reduction Reaction: Activity of Structurally Well Defined Au_xPt_{11x}/Pt(111) Monolayer Surface Alloys. *J. Electroanal. Chem.* **2014**, *716*, 71−79.
(41) Engstfeld, A. K.; Hoster, H. E.; Behm, R. J. Formation, Atomic Distribution and Mixing Energy in Two-Dimensional Ag_xPd_{1-x} Surface Alloys on Pd(111). *Phys. Chem. Chem. Phys.* **2012**, *14*, 10754−10761.
(42) Ma, Y.; Bansmann, J.; Diemant, T.; Behm, R. J. Formation, Stability and CO Adsorption Properties of PdAg/Pd(111) Surface Alloys. *Surf. Sci.* **2009**, *603*, 1046−1054.
(43) Ma, Y.; Diemant, T.; Bansmann, J.; Behm, R. J. The Interaction of CO With PdAg/Pd(111) Surface Alloys-A Case Study of Ensemble Effects on a Bimetallic Surface. *Phys. Chem. Chem. Phys.* **2011**, *13*, 10741−10754.
(44) Farkas, A. P.; Diemant, T.; Bansmann, J.; Behm, R. J. The Adsorption of Oxygen and Coadsorption of CO and Oxygen on PdAg/Pd(111) Surface Alloys. *ChemPhysChem* **2012**, *13*, 3516−3525.
(45) Mancera, L. A.; Behm, R. J.; Groß, A. Structure and Local Reactivity of PdAg/Pd(111) Surface Alloys. *Phys. Chem. Chem. Phys.* **2013**, *15*, 1497−1508.
(46) Behm, R. J. Interaction of Hydrogen With Bimetallic Surfaces. *Z. Phys. Chem.* **2009**, *223*, 9−36.
(47) Takehiro, N.; Liu, P.; Bergbreiter, A.; Nørskov, J. K.; Behm, R. J. Hydrogen Adsorption on Bimetallic PdAu(111) Surface Alloys: Minimum Adsorption Ensemble, Ligand and Ensemble Effects, and Ensemble Confinement. *Phys. Chem. Chem. Phys.* **2014**, *16*, 23930−23942.
(48) Christmann, K. Interaction of Hydrogen With Solid Surfaces. *Surf. Sci. Rep.* **1988**, *9*, 1−163.
(49) Smentkowski, V. S.; Yates, J. T., Jr A Multipurpose Quadrupole Mass Spectrometer Detector for Surface Kinetic and Absolute Surface Coverage Measurements. *J. Vac. Sci. Technol. A* **1989**, *7*, 3325−3328.
(50) Kresse, G.; Furthmüller, J. Efficient Iterative Schemes for Ab Initio Total-Energy Calculations Using a Plane-Wave Basis Set. *Phys. Rev. B* **1996**, *54*, 11169−11186.
(51) Perdew, J. P.; Burke, K.; Ernzerhof, M. Generalized Gradient Approximation Made Simple. *Phys. Rev. Lett.* **1996**, *77*, 3865−3868.
(52) Blöchl, P. E. Projector Augmented-Wave Method. *Phys. Rev. B* **1994**, *50*, 17953−17979.
(53) Kresse, G.; Furthmüller, J. Efficiency of Ab-Initio Total Energy Calculations for Metals and Semiconductors Using a Plane-Wave Basis Set. *Comput. Mater. Sci.* **1996**, *6*, 15−50.
(54) Kresse, G.; Joubert, D. From Ultrasoft Pseudopotentials to the Projector Augmented-Wave Method. *Phys. Rev. B* **1999**, *59*, 1758−1775.
(55) Mills, G.; Jónsson, H.; Schenter, G. K. Reversible Work Transition State Theory: Application to Dissociative Adsorption of Hydrogen. *Surf. Sci.* **1995**, *324*, 305−337.
(56) Jónsson, H.; Mills, G.; Jacobsen, K. W. In *Classical and Quantum Dynamics in Condensed Phase Simulations*; Berne, B. J., Ciccotti, G., Coke, D. F., Eds.; World Scientific: Singapore, 1998; pp 385−404.
(57) Noordermeer, A.; Kok, G. A.; Nieuwenhuys, B. E. A Comparative Study of the Behaviour of the PdAg(111) and Pd(111) Surfaces Towards the Interaction With Hydrogen and Carbon Monoxide. *Surf. Sci.* **1986**, *165*, 375−392.
(58) Tamtögl, A.; Kratzer, M.; Killman, J.; Winkler, A. Adsorption/Desorption of H_2 and CO on Zn-Modified Pd(111). *J. Chem. Phys.* **2008**, *129*, 224706.
(59) Ozawa, N.; Arboleda, N. B.; Nakanishi, H.; Kasai, H. First Principles Study of Hydrogen Atom Adsorption and Diffusion on Pd3Ag(111) Surface and in Its Subsurface. *Surf. Sci.* **2008**, *602*, 859−863.
(60) Schnur, S.; Groß, A. Challenges in the First-Principles Description of Reactions in Electrocatalysis. *Catal. Today* **2011**, *165*, 129−137.
(61) Roudgar, A.; Groß, A. Local Reactivity of Metal Overlayers: Density Functional Theory Calculations of Pd on Au. *Phys. Rev. B* **2003**, *67*, 033409.
(62) Gohda, Y.; Groß, A. Structure-Reactivity Relationships for Bimetallic Electrodes: Pt Overlayers and PtAu Surface Alloys on Au(111). *J. Electroanal. Chem.* **2007**, *607*, 47−53.
(63) Liu, P.; Nørskov, J. K. Ligand and Ensemble Effects in Adsorption on Alloy Surfaces. *Phys. Chem. Chem. Phys.* **2001**, *3*, 3814−3818.
(64) Mancera, L. A.; Behm, R. J.; Groß, A. Structure and Local Reactivity of PdAg/Pd(111) Surface Alloys. *Phys. Chem. Chem. Phys.* **2013**, *15*, 1497−1508.

(65) Ruff, M.; Takehiro, N.; Liu, P.; Nørskov, J. K.; Behm, R. J. Size-Specific Chemistry on Bimetallic Surfaces: A Combined Experimental and Theoretical Study. *ChemPhysChem* **2007**, *8*, 2068−2071.
(66) Diemant, T.; Hager, T.; Hoster, H. E.; Rauscher, H.; Behm, R. J. Hydrogen Adsorption and Coadsorption With CO on Well-Defined Bimetallic PtRu Surfaces - A Model Study on the CO Tolerance of Bimetallic PtRu Anode Catalysts in Low Temperature Polymer Electrolyte Fuel Cells. *Surf. Sci.* **2003**, *541*, 137−146.
(67) Rauscher, H.; Hager, T.; Diemant, T.; Hoster, H.; Buatier de Mongeot, F.; Behm, R. J. Interaction of CO With Atomically Well-Defined Pt_xRu_y/Ru(0001) Surface Alloys. *Surf. Sci.* **2007**, *601*, 4608−4619.
(68) Diemant, T.; Rauscher, H.; Behm, R. J. Interaction of D_2 With Atomically Well-Defined PtRu/Ru(0001) Surface Alloys. *J. Phys. Chem. C* **2008**, *112*, 8381−8390.
(69) Schmidt, P. K.; Christmann, K.; Kresse, G.; Hafner, J.; Lischka, M.; Groß, A. Coexistence of Atomic and Molecular Chemisorption States: H_2/Pd(210). *Phys. Rev. Lett.* **2001**, *87*, 096103.
(70) Lischka, M.; Groß, A. Hydrogen Adsorption on an Open Metal Surface: H_2/Pd(210). *Phys. Rev. B* **2002**, *65*, 075420.
(71) Lide, D. R., Ed. *Handbook of Chemistry and Physics*, 87th ed.; CRC Press, 2006.
(72) Hammer, B.; Nørskov, J. K. Theoretical Surface Science and Catalysis-Calculations and Concepts. *Adv. Catal.* **2000**, *45*, 71−129.
(73) Han, Y.-F.; Kumar, D.; Sivadinarayana, C.; Clearfield, A.; Goodman, D. W. The Formation of PdC_x Over Pd-Based Catalysts in Vapor-Phase Vinyl Acetate Synthesis: Does a Pd-Au Alloy Catalyst Resist Carbide Formation? *Catal. Lett.* **2004**, *94*, 131−134.
(74) Han, Y.-F.; Wang, J.-H.; Kumar, D.; Yan, Z.; Goodman, D. W. A Kinetic Study of Vinyl Acetate Synthesis Over Pd-Based Catalysts: Kinetics of Vinyl Acetate Synthesis Over Pd-Au/SiO2 and Pd/SiO2 Catalysts. *J. Catal.* **2005**, *232*, 467−475.
(75) Chen, M. S.; Luo, K.; Wei, T.; Yan, Z.; Kumar, D.; Yi, C. W.; Goodman, D. W. The Nature of the Active Sites for Vinyl Acetate Synthesis Over Pd-Au. *Catal. Today* **2006**, *117*, 37−45.
(76) Chen, M.; Goodman, D. W. Promotional Effects of Au in Pd-Au Catalysts for Vinyl Acetate Synthesis. *Chin. J. Catal.* **2008**, *29*, 1178−1186.
(77) Gao, F.; Goodman, D. W. Model Catalysts: Simulating the Complexities of Heterogeneous Catalysts. *Annu. Rev. Phys. Chem.* **2012**, *63*, 265−286.